

Entropy Rectifying Guidance for Diffusion and Flow Models

Tariq Berrada Ifriqi^{1,2}, Adriana Romero-Soriano^{1,3,4,5}, Michal Drozdal¹, Jakob Verbeek¹, Karteek Alahari²

¹FAIR at Meta, ²Univ. Grenoble Alpes, Inria, CNRS, Grenoble INP, LJK, France, ³McGill University, ⁴Mila, Quebec AI institute, ⁵Canada CIFAR AI chair

Guidance techniques are commonly used in diffusion and flow models to improve image quality and consistency for conditional generative tasks such as class-conditional and text-to-image generation. In particular, classifier-free guidance (CFG) — the most widely adopted guidance technique — contrasts conditional and unconditional predictions to improve the generated images. This results, however, in trade-offs across quality, diversity and consistency, improving some at the expense of others. While recent work has shown that it is possible to disentangle these factors to some extent, such methods come with an overhead of requiring an additional (weaker) model, or require more forward passes per sampling step. In this paper, we propose Entropy Rectifying Guidance (ERG), a simple and effective guidance mechanism based on inference-time changes in the attention mechanism of state-of-the-art diffusion transformer architectures, which allows for simultaneous improvements over image quality, diversity and prompt consistency. ERG is more general than CFG and similar guidance techniques, as it extends to unconditional sampling. ERG results in significant improvements in various generation tasks such as text-to-image, class-conditional and unconditional image generation. We also show that ERG can be seamlessly combined with other recent guidance methods such as CADs and APG, further boosting generation performance.

Correspondence: First Author at tariqberrada@meta.com



1 Introduction

Diffusion (Sohl-Dickstein et al., 2015; Ho et al., 2020; Song et al., 2021; Dhariwal and Nichol, 2021) and flow models (Lipman et al., 2023; Ma et al., 2024; Esser et al., 2024) are state-of-the-art generative modeling tools for various modalities, ranging from images (Rombach et al., 2022; Podell et al., 2024; Chen et al., 2024; Esser et al., 2024), audio (Wang et al., 2023; Levy et al., 2023), and video (Jin et al., 2025; Polyak et al., 2024). These models generate data by starting with a simple prior and iteratively removing noise – a process called “denoising”. See Kingma and Gao (2023); Lipman et al. (2023) for details on diffusion and flow matching. These models can be conditioned on various inputs to control the generative process, e.g., in text-to-image models. Guidance techniques such as classifier guidance (Dhariwal and Nichol, 2021) and classifier-free guidance (Ho and Salimans, 2021) are commonly used to improve sample quality and consistency with input conditioning. In the sampling process, these techniques combine a conditional signal with an unconditional one, and control the strength of conditioning through a scaling parameter. Although such guidance techniques are a crucial component in achieving state-of-the-art results, they are also known to affect the diversity of generated samples given a particular prompt (Sadat et al., 2024; Karras et al., 2024; Kynkäänniemi et al., 2024; Saharia et al., 2022). Moreover, too high guidance scales may lead to overly saturated images, affecting the quality of generated images (Saharia et al., 2022). An extensive analysis on the trade-offs of image generation quality, diversity, and consistency was presented by Astolfi et al. (2024). To mitigate quality-diversity-consistency trade-offs, more advanced guidance techniques have recently been proposed (Sadat et al., 2025; Karras et al., 2024). Most guidance approaches require spending part of the training cycles on unconditional generation for the guidance to work well (Sadat et al., 2025; Ho and Salimans, 2021), even if unconditional generation is not a goal in itself. They often rely on another model with weaker performance than the main model, thereby increasing memory requirements (Karras et al., 2024), or are not applicable to unconditional image generation (Sadat et al., 2025; Ho and Salimans, 2021).

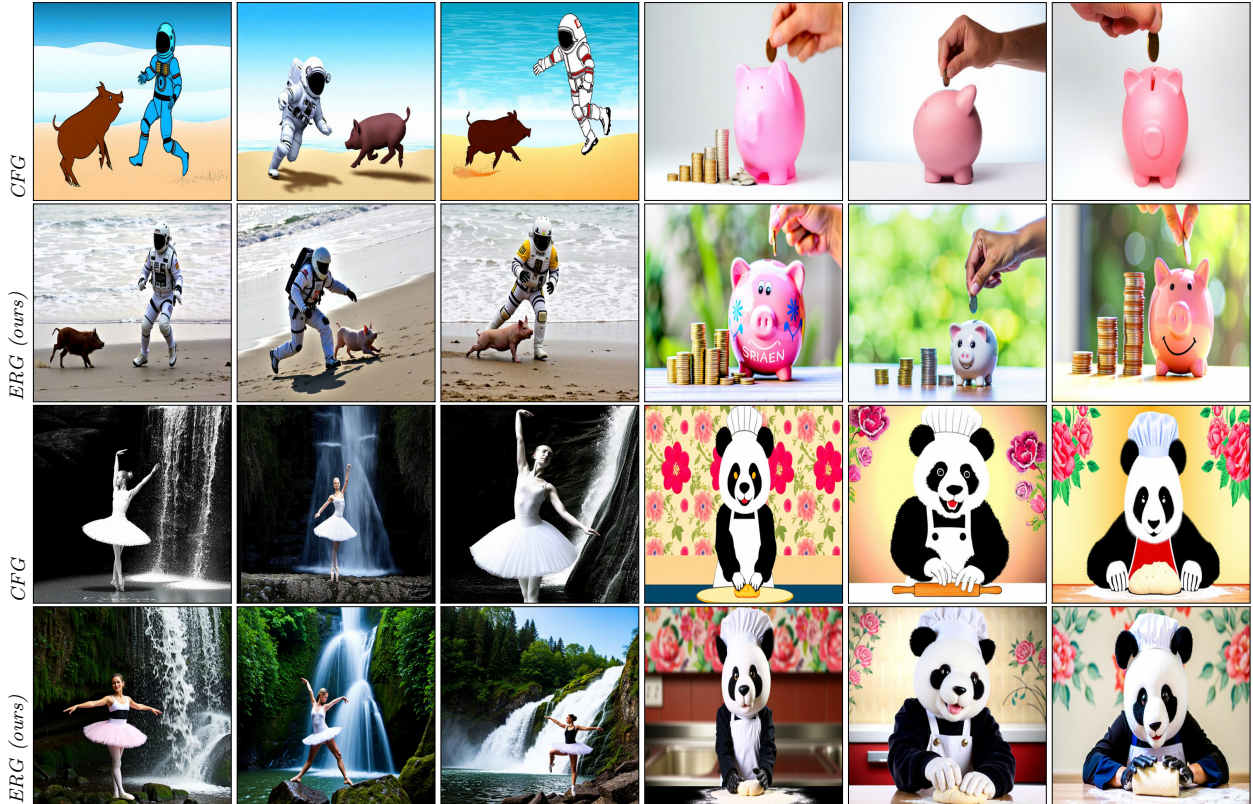


Figure 1 Qualitative comparison of classifier-free guidance (CFG) and our Entropy Rectifying Guidance (ERG). The images generated using ERG (bottom rows) exhibit greater quality and diversity than standard CFG. Images are generated using 50 Euler steps; each column corresponds to a different random seed for the generations.

In our work, we build upon the work of [Karras et al. \(2024\)](#) and [Hong \(2024\)](#) and propose a simple and effective method to obtain *both* a *strong* and a *weak* predictive signal from a *single model* that leverages attention layers, where the model may be conditional or unconditional. In particular, our method uses the Hopfield energy formulation of attention ([Ramsauer et al., 2021](#)) and applies a temperature scaling to the softmax function of the attention layers in order to obtain the weak predictive signal. This scaling does not require any adaptations in model training, and may be applied to pre-trained denoising models, as well as their accompanying text encoders. Moreover, motivated by this energy interpretation of attention layers ([Hong, 2024](#); [Ramsauer et al., 2021](#)), we also consider iterative re-application of attention layers, and rescaling the residual attention update. Our experiments show that manipulating the attention layers in this manner results in simultaneous improvements in sample quality, diversity, and consistency, contrary to the trade-offs observed by [Astolfi et al. \(2024\)](#) for classifier-free guidance.

In summary, our contributions are the following:

1. We propose Entropy Rectifying Guidance (ERG), a guidance mechanism based on modifying the energy landscape of the attention layers.
2. Since our guidance mechanism does not require unconditional inference, it is directly applicable to any attention-based diffusion or flow model, including unconditional, class-conditional, and text-to-image models.
3. Experimentally, we find that our guidance method significantly improves image quality *and* diversity while retaining the same prompt consistency as the standard classifier-free guidance (+30 points in density, +4 points in VQAScore) on COCO@512 using our 1.9 text-to-image image.

2 Related work and background

In this section, we briefly review background material on diffusion models, and related work on guidance techniques to improve sampling as well as the Hopfield energy formulation of attention.

2.1 Diffusion and flow matching models

Diffusion models (Sohl-Dickstein et al., 2015; Ho et al., 2020; Song et al., 2021) form a flexible class of generative models whose underlying principle is to map samples ϵ from a trivial unit Gaussian prior $p_0 = \mathcal{N}(0, \mathbf{I})$ to samples from a learned model p_1 of the data distribution. The forward process is defined as:

$$\mathbf{x}_t = \alpha_t \mathbf{x}_1 + \sigma_t \epsilon, \quad \text{with } t \in [0, 1], \quad (1)$$

where $x_1 \sim p_1$, and α_t is a decreasing function of “time” t while σ_t an increasing function of t .

Flow matching methods (Lipman et al., 2023) assume that $\alpha_0 = \sigma_1 = 1$ and $\alpha_1 = \sigma_0 = 0$. Using these assumptions, during the reverse process \mathbf{x}_t interpolates between ϵ at $t = 0$ and \mathbf{x}_1 at $t = 1$. In contrast, score-based diffusion models (Ho et al., 2020; Dhariwal and Nichol, 2021) set α_t and σ_t implicitly through different formulations of stochastic differential equations (SDE) where $\mathcal{N}(0, \mathbf{I})$ is the equilibrium distribution. Additionally, they consider $t \in [0, T]$ with T large enough so that \mathbf{x}_T is approximately distributed as a unit Gaussian random variable.

2.2 Guidance mechanisms

Classifier guidance. To enable high quality conditional generation, Dhariwal and Nichol (2021) proposed to guide the sampling process by leveraging gradients from pre-trained auxiliary classifier $p(c|\mathbf{x})$ in each reverse denoising step. They use the classifier to define the (scaled) joint score function as:

$$\nabla_{\mathbf{x}_t} \log p(\mathbf{x}_t, c) = \nabla_{\mathbf{x}_t} \log p(\mathbf{x}_t) + w \nabla_{\mathbf{x}_t} \log p(c|\mathbf{x}_t), \quad (2)$$

where $p(\mathbf{x}_t)$ is an unconditional data model, and w is a scalar parameter regulating the strength of the classifier guidance. While classifier guidance allows to improve input consistency and image quality (at the expense of diversity), it requires an auxiliary classification model that is robust to inputs \mathbf{x}_t with varying amounts of noise.

Classifier-free guidance. To avoid the need for an auxiliary noise-robust classifier, Ho and Salimans (2021) proposed classifier-free guidance (CFG). In this case, during the training process, two generative models are learned, one conditional $p(\mathbf{x}|c)$ and one unconditional $p(\mathbf{x}|\emptyset)$. In practice, the unconditional model is trained by dropping conditioning information with a small probability. The score function used for sampling is extrapolated towards the conditional prediction and away from the unconditional prediction:

$$\nabla_{\mathbf{x}}^{\text{CFG}} \log p(\mathbf{x}|c) = w \nabla_{\mathbf{x}} \log p(\mathbf{x}|c) + (1 - w) \nabla_{\mathbf{x}} \log p(\mathbf{x}|\emptyset). \quad (3)$$

While CFG improves image quality and input consistency with respect to classifier guidance, it tends to come at the cost of a reduction in diversity (Astolfi et al., 2024; Ho and Salimans, 2021; Sadat et al., 2024). Moreover, CFG often leads to generation artifacts, such as over-saturation as the guidance scale grows (Sadat et al., 2025).

Advanced guidance techniques. Several improved variants of classifier-free guidance have been proposed recently. Hong et al. (2023) presented Self-Attention Guidance (SAG), a guidance mechanism based on feeding a modified intermediate sample \mathbf{x}_t when performing inference for unconditional prediction. The modification consists in blurring \mathbf{x}_t in regions that are most attended to by the model’s self-attention. This method has been developed for the UNet architecture, hence applying it to more recent diffusion transformer architectures requires a hyperparameter search to understand which attention layers should be used for this method.

Smoothed energy guidance (SEG) (Hong, 2024) contrasts conditional prediction with a “weaker” conditional prediction obtained by altering the attention’s softmax energy with a Gaussian kernel applied to queries. This

method is developed for U-Net-style architectures and the softmax alteration applies to the self-attention layers in the middle block of the U-Net. Note that SEG does not rely on the difference between conditional and unconditional terms, and applies to both conditional and unconditional sampling. In the conditional case, SEG uses a linear combination of the conditional, unconditional, and energy-smoothed unconditional prediction, whereas in our approach we only use the conditional and smoothed conditional term. Thus, SEG requires an additional function evaluation with respect to ERG for conditional inference. For unconditional inference, both approaches require only two function evaluations. In a similar spirit, [Ahn et al. \(2024\)](#) propose a guidance method based on manipulating the attention mechanism, by replacing the attention matrix with an identity mapping inside the denoiser U-Net.

[Karras et al. \(2024\)](#) explore using a smaller/weaker version of the same conditional model for classifier-free guidance, resulting in better diversity and image quality. Like ours, their approach can also be applied to unconditional sampling. However, their method requires access to an earlier checkpoint of the model or, for best results, training a separate model with lower capacity, as well as accessing two models when sampling, which may increase the memory footprint by a factor two.

Rather than considering modifications of the unconditional model term, [Sadat et al. \(2024\)](#) proposed the “condition-annealed diffusion sampler” (CADS) to increase the diversity of generations while maintaining sample quality. This is achieved by adding Gaussian noise to the conditioning tokens during inference, using a piecewise-linear decreasing schedule on the noise amplitude. [Sadat et al. \(2025\)](#) propose “adaptive projected guidance” (APG), a variant of classifier-free guidance that resolves the over-saturation problem by emphasizing guidance orthogonal to the conditional prediction, rescaling the guidance term, and introducing a negative momentum term. The latter two approaches can be easily combined with our approach, and we consider such combinations in our experiments.

Lastly, several works ([Kynkäänniemi et al., 2024](#); [Pavasovic et al., 2025](#); [Wang et al., 2024](#)) explore non-constant weight schedules for CFG. Such methods are complementary to our work, as our method only operates at the architecture level by rectifying the attention updates. Although they therefore could be combined with our approach, we defer this to future work.

2.3 Hopfield energy formulation of attention

The Hopfield network ([Hopfield, 1982](#)) is a dense associative memory model that aims to associate an input with its most similar pattern. More specifically, it constructs an energy function to model an energy landscape that contains basins of attraction around the desired patterns. Modern Hopfield energy networks ([Ramsauer et al., 2021](#)) introduce a new family of energy functions that improve the storage capacity of the model and make it compatible with continuous embeddings. Specifically, the following energy functional matches a continuous d -dimensional state (query) pattern $\boldsymbol{\xi} \in \mathbb{R}^d$ with N stored (key) patterns $\mathbf{X} = (\mathbf{x}_1, \dots, \mathbf{x}_N) \in \mathbb{R}^{d \times N}$ as:

$$E(\boldsymbol{\xi}; \mathbf{X}) = \frac{1}{2} \boldsymbol{\xi}^\top \boldsymbol{\xi} - \text{LogSumExp}(\mathbf{X}^\top \boldsymbol{\xi}, \beta), \quad (4)$$

where $\text{LogSumExp}(\mathbf{x}, \beta) = \beta^{-1} \log(\sum_{i=1} \exp(x_i))$, where x_i are the elements of the vector \mathbf{x} , and β a scalar hyperparameter defining the sharpness of the approximation of the maximum in the LogSumExp operation. Intuitively, the first term imposes a finite norm on the queries while the second term measures the alignment between the state patterns (queries) and stored patterns (keys). Using the Concave-Convex Procedure (CCCP) ([Yuille and Rangarajan, 2003](#)), an iterative update rule, which converges to the global minima of the energy, can be derived as:

$$\boldsymbol{\xi}_{l+1} = \mathbf{X} \text{SoftMax}(\beta \mathbf{X}^\top \boldsymbol{\xi}_l), \quad (5)$$

where $\text{SoftMax}(\mathbf{x}) = \exp(\mathbf{x} - \text{LogSumExp}(\mathbf{x}, 1))$. Equivalently, each iterative update step can be seen as a gradient update in the negative direction of the energy:

$$\nabla_{\boldsymbol{\xi}} E(\boldsymbol{\xi}; \mathbf{X}) = \boldsymbol{\xi} - \mathbf{X} \text{SoftMax}(\beta \mathbf{X}^\top \boldsymbol{\xi}). \quad (6)$$

Taking a gradient descent step on this energy landscape with a step size γ results in an update of the form $\boldsymbol{\xi}_{l+1} = \boldsymbol{\xi}_l - \gamma (\boldsymbol{\xi}_l - \mathbf{X} \text{softmax}(\beta \mathbf{X}^\top \boldsymbol{\xi}_l))$, and for $\gamma = 1$ we recover the CCCP update.

[Ramsauer et al. \(2021\)](#) show that the CCCP update is related to the standard attention operation as follows. Assuming there are S state (query) patterns, and N stored (key) patterns that can be mapped to keys,

queries and values using linear transformations, the state pattern can be obtained through a concatenation: $\Xi = [\xi_1, \dots, \xi_S] \in \mathbb{R}^{d \times S}$. Then the attention map is given by $\Xi_{l+1} = \mathbf{X} \text{softmax}(\mathbf{X}^\top \Xi_l)$. The keys, queries and values are obtained via linear projections as $\mathbf{K} = \mathbf{X}W_K^\top \in \mathbb{R}^{N \times d}$, $\mathbf{V} = \mathbf{X}W_V^\top \in \mathbb{R}^{N \times d}$ and $\mathbf{Q} = \Xi_{l+1}W_Q^\top \in \mathbb{R}^{S \times d}$, respectively. By setting $\beta = \frac{1}{\sqrt{d}}$ and substituting this into Equation (5), we obtain:

$$\mathbf{Q}_{l+1} = \text{SoftMax}\left(\frac{\mathbf{Q}\mathbf{K}^\top}{\sqrt{d}}\right)\mathbf{K} \quad (7)$$

$$= \text{SoftMax}\left(\frac{\mathbf{Q}\mathbf{K}^\top}{\sqrt{d}}\right)\mathbf{V}(W_KW_V^{-1})^\top. \quad (8)$$

Hence, we observe the equation of attention up to a linear transformation, which provides an interpretation of the attention mechanism through the Hopfield energy lens. Such a formulation has been used in the Energy Based Cross-Attention method (EBCA) (Park et al., 2024) for adaptive context control in order to incorporate additional contexts into the generative process of a conditional diffusion model.

3 Guidance via Entropy Rectification

Similarly to previous approaches (Ho and Salimans, 2021; Hong, 2024; Karras et al., 2024), our approach is based on contrasting the denoising estimate with a less powerful one. In particular, using the Hopfield energy interpretation of attention in Equation (4), we manipulate the energy landscape of the attention layer, by rectifying the entropy of the associations in the attention operation. The modified attention layers lead to lower quality predictions, which are used as the contrasting term for guidance. This approach does not require a second model and can be used for both conditional and unconditional sampling. We refer to our approach as Entropy Rectifying Guidance (ERG).

3.1 Manipulating the energy landscape

Our method manipulates the energy landscapes by introducing two new test-time hyperparameters, α and τ in the energy function:

$$E(\xi; \mathbf{X}) = \frac{1}{2}\xi^\top \xi - \alpha \cdot \text{logsumexp}(\mathbf{X}^\top \xi, \tau \cdot \beta). \quad (9)$$

The temperature rescaling parameter τ controls the sharpness of the softmax attention, and α the relative importance of the similarity between the state matching term compared to the norm of the state patterns. Temperature rescaling with τ is similar to the Gaussian blurring of the attention maps introduced in SEG (Hong, 2024), but allows for non-local smoothing of the attention layers. Additionally, the view of the attention layer as a CCCP update of the energy function, allows for consideration of different methods to minimize the energy landscape. For instance, taking K gradient descent steps with step size γ , as illustrated in Algorithm 1. Using different settings of the hyperparameters α , γ , and τ allows us to manipulate the energy landscape modeling the attention operation, and obtain noise estimates that deviate from the trained model. We expect these to be weaker estimates compared to those provided by the model, as it was trained with standard attention layers, i.e. with $\alpha = \gamma = \tau = 1$. When applying this rectification mechanism to the denoiser model, we refer to the method as image-ERG, or I-ERG for short. In particular, we apply it to the negative/unconditional prediction part of the classifier-free guidance, only on certain layers of the network that will be defined subsequently. Additionally, we impose a kickoff threshold κ on the time steps in which guidance is applied.

Algorithm 1 Multi-step Entropy Rectifying Guidance.

Require: $K \in \mathbb{N}$ number of gradient update steps.

Require: $\gamma > 0$ step size.

Require: $\alpha \in \mathbb{R}$ State pattern matching weight.

Require: $\tau > 0$ attention temperature.

Require: $\mathbf{K}, \mathbf{V} \in \mathbb{R}^{d \times N}$ keys and values.

Require: $\mathbf{Q} \in \mathbb{R}^{d \times S}$ queries.

$k \leftarrow 0$

while $k < K$ **do**

$\mathbf{Q} \leftarrow \mathbf{Q} - \gamma \left(\mathbf{Q} - \alpha \cdot \text{softmax}(\tau \cdot \beta \mathbf{Q}\mathbf{K}^\top) \mathbf{V} \right)$ ¹

$k \leftarrow k + 1$

end while

¹ $\beta = \frac{1}{\sqrt{d}}$ is the default temperature of the attention attention update.

3.2 Manipulating the energy of the text encoder

Besides the image denoising model, we can also manipulate the energy landscape of attention-based text encoders to obtain a weak version of the conditional embeddings. Let c be the text prompt that is used as conditioning. The text tokens are obtained by feeding the prompt to the text encoder: $\text{Enc}(c) \in \mathbb{R}^{d_t}$, such as Llama (Grattafiori et al., 2024) or T5 (Chung et al., 2022). Text tokens are then fed to the denoiser model through cross-attention layers.

To obtain a contrasting signal for guidance, we manipulate the energy landscape in the self-attention layers of the text encoder following Algorithm 1. More specifically, for every self-attention layer in the text encoder, we introduce a temperature hyperparameter in the attention map of every softmax. This enables us to reduce the certainty with which keys and queries are being matched, resulting in less precise tokens at the output. For the remainder of the manuscript, we refer to this method condition-ERG, or C-ERG for short. For simplicity reasons, we only consider changing the temperature but not the step size γ and pattern matching weight α .

3.3 Guidance update

When combining the energy modulations in the text-encoder and denoising model, we obtain our Entropy Rectifying Guidance (ERG) update:

$$\Delta_{\text{ERG}}(\mathbf{x}, c, t; \Theta_\xi) = w \cdot D(\mathbf{x}, \phi_c, t) + (1 - w) \cdot D^\xi(\mathbf{x}, \phi_c^\tau, t; \Theta_\xi), \quad (10)$$

where D is the learned denoiser model with parameters Θ that are omitted for simplicity, D^ξ is the denoiser model where the attention layers have been replaced by the modified version presented in Equation (9), and Θ_ξ the set of hyperparameters introduced by our method. ϕ_c are hidden states of the text encoder while ϕ_c^τ is the hidden states of the text encoder obtained with a modified energy landscape in the attention layers. Compared to the standard CFG, the main differences are that we replace the unconditional text embeddings with conditional embeddings obtained with the entropy-rectified attention mechanism (C-ERG). Similarly, the denoiser model used for the negative/unconditional predictions is also obtained with a rectified attention mechanism (I-ERG). Finally, the denoiser level updates are only applied after a certain point during sampling in order to not overly penalize the negative components of the ERG update at the start of sampling.

Note that our approach can be combined with other approaches, e.g., CADs (Sadat et al., 2024) and APG (Sadat et al., 2025). We will explore such combinations in our experiments.

4 Experimental evaluation

4.1 Experimental setup

Datasets and architectures. We experiment with class-conditional and text-to-image models. Both models are trained at 512×512 image resolution using the rectified flow-matching paradigm (Lipman et al., 2023; Esser et al., 2024). We train class-conditional models on a faceblurred version of ImageNet (Deng et al., 2009). For the class-conditional setting, we experiment with the XL/2 variant of the DiT architecture (Peebles and Xie, 2023) which is composed of 28 attention blocks with hidden dimension of 1152, resulting in 790M parameters; in this setting we evaluate models at both 256 and 512 resolutions. For the text-to-image model, we use an architecture similar to MMDiT (Esser et al., 2024), and train on a mix of a proprietary dataset of 320M text-image pairs and YFCC100M, where all faces in YFCC100M have been blurred. Similarly to MMDiT (Esser et al., 2024), the model uses a mix of different text encoders: Llama3-8b (Grattafiori et al., 2024) and Flan-T5-XL (Chung et al., 2022). During training, each of the text encoders is disabled with a probability of $\sqrt{0.1}$, so that the probability of both encoders being disabled is around 10%. We enable both text encoders during inference time. The architecture of the model is made of 38 blocks with a hidden dimension of 1536, resulting in approx 1.9B parameters. For both datasets, we recaption the images using both Florence-2 Large (Xiao et al., 2024) to obtain medium-length captions and PaliGemma-3b (Beyer et al., 2024) for shorter COCO-style captions. Additional techniques to improve training efficiency of this model, such as conditioning mechanisms and pre-training strategies, were adopted from Berrada et al. (2024). For

Table 1 Comparison of our Entropy Rectifying Guidance (ERG) with other guidance approaches. Conducted for text-to-image generation using the COCO’14 validation data. Scores obtained by the hyper-parameter setting achieving the optimal mean rank across the pool of combinations. We compare ERG to other state-of-the-art guidance approaches and mark the best result in each column in bold in the top part of the table. In the bottom part of the table we evaluate combinations of ERG with APG and CADs, and bold results when they surpass the results reported in the upper part of the table.

| Metric \ Guidance | FID (↓) | Precision (↑) | Recall (↑) | Density (↑) | Coverage (↑) | CLIPScore (↑) | VQAScore (↑) | NFE (↓) |
|------------------------------------|--------------|---------------|--------------|---------------|--------------|---------------|--------------|---------|
| CFG (Ho and Salimans, 2021) | 12.81 | 65.71 | 43.95 | 98.24 | 71.12 | 26.45 | 70.15 | 2 |
| APG (Sadat et al., 2025) | 11.88 | 66.34 | 45.15 | 104.07 | 73.06 | 26.54 | 72.47 | 2 |
| CADs (Sadat et al., 2024) | 11.93 | 66.42 | 45.75 | 101.01 | 72.99 | 26.76 | 73.36 | 2 |
| PAG* (Ahn et al., 2024) | 12.75 | 66.42 | 43.94 | 107.21 | 72.20 | 26.80 | 73.32 | 2 |
| SAG* (Hong et al. (2023)) | 11.68 | 64.97 | 47.98 | 103.58 | 72.74 | 26.81 | 72.16 | 2 |
| SEG* (Hong, 2024) | 16.87 | 61.22 | 36.88 | 87.77 | 61.91 | 26.86 | 73.59 | 3 |
| AutoGuidance (Karras et al., 2024) | 16.62 | 61.48 | 34.60 | 87.02 | 62.75 | 26.59 | 73.53 | 2 |
| ERG (ours) | 13.62 | 70.92 | 41.43 | 120.25 | 73.21 | 26.86 | 73.96 | 2 |
| ERG (ours) + APG | 11.37 | 69.50 | 50.25 | 115.08 | 80.50 | 26.74 | 73.55 | 2 |
| ERG (ours) + CADs | 12.87 | 72.72 | 38.89 | 128.54 | 76.23 | 26.75 | 73.45 | 2 |

the class-conditional model we use the asymmetric autoencoder of Zhu et al. (2023), while for the larger text-to-image model we use the SD3 autoencoder which has latent representation with 16 channels.

Metrics. We consider metrics for quality, diversity, and consistency (Astolfi et al., 2024). We measure *sample quality* with FID (Heusel et al., 2017), precision (Kynkäänniemi et al., 2019) and density (Naeem et al., 2020); *sample diversity* is measured with recall (Kynkäänniemi et al., 2019), coverage (Naeem et al., 2020) and FID; and *input consistency* is measured with CLIPScore (Hessel et al., 2021) and VQAScore (Lin et al., 2024).

For evaluation of text-to-image and unconditional generation, we use the 40k COCO’14 validation image-caption pairs. For the class-conditional models, we sample 50 images for each of the 1,000 ImageNet classes and use the ImageNet validation set as a reference. All evaluated models are sampled using the Euler method with 50 sampling steps. We use the EvalGIM (Hall et al., 2024) library for all evaluations.

Baselines. In addition to the standard classifier-free guidance, we compare our method with Condition-Annealed Diffusion Sampler (CADs) (Sadat et al., 2024), Adaptive Projected Guidance (APG) (Sadat et al., 2025), Smooth Energy Guidance (SEG) (Hong, 2024) and Auto-Guidance (Karras et al., 2024). For APG, we follow the recommendations from the paper and set $\gamma_{\text{APG}} = -0.5$, $\eta_{\text{APG}} = 0.0$, $r_{\text{APG}} = 5.0$. For CADs, we perform a grid search over $\tau_1^{\text{CADs}} \in [0.6, 0.8]$, $\tau_2^{\text{CADs}} \in [0.8, 1.0]$, $s^{\text{CADs}} \in [0.25, 1.0]$, $\psi^{\text{CADs}} = 1.0$. To ensure a fair comparison, we select the best performing guidance strength for baselines as well as our method using the rank-scoring algorithm defined in the appendix, see Appendix A.1 for details. Note that this is different from reporting the optimal score achieved for each metric, as such a report might not correspond to any particular run because of inherent trade-offs between the different facets of the generations.

Since SAG, PAG and SEG were developed specifically for the UNet architecture, we adapt these method for diffusion transformers (Peebles and Xie, 2023) by applying the method in the attention layers of the middle blocks of the transformer; we refer to these methods with an asterisk superscript *. Additional details on the choice of layers are provided in Appendix B.4. For AutoGuidance, we follow the recommendations from the paper and use an earlier checkpoint of the same model, at approximately 1/16-th of the training, as the weaker model.

4.2 Main experimental results

Throughout our experiments, we modify attention layers in both the text encoder (C-ERG) and the image denoising model (I-ERG), unless specified otherwise.

Text-to-image generation. In Table 1, we compare our Entropy Rectifying Guidance with different guidance mechanisms from the literature on the text-to-image generation task. Our proposed ERG approach demonstrates competitive performance across various metrics for text-to-image generation on the COCO’14 validation set, outperforming baselines such as CFG, SAG, PAG and SEG* in most metrics. Specifically, ERG considerably boosts image quality as reported in quality metrics (e.g., +22 for density and +5 for precision

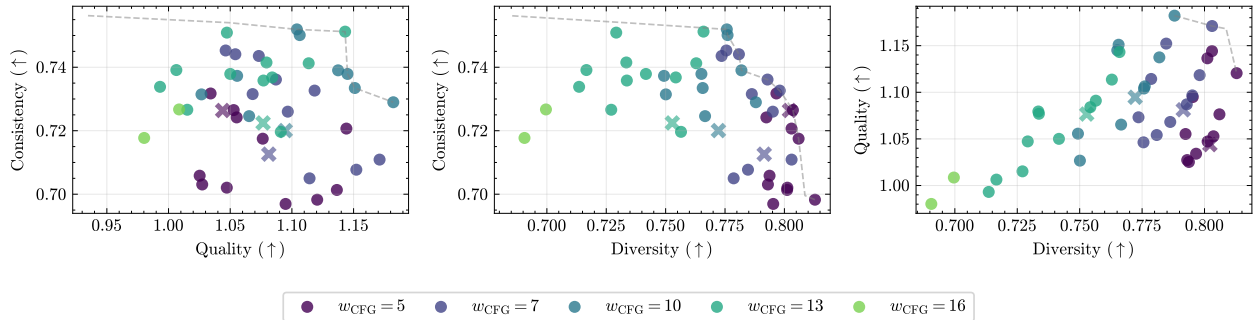


Figure 2 Pareto fronts on consistency-diversity-quality for text-to-image generation. Metrics computed on COCO using ERG + APG, points with a \times sign correspond to APG. We sweep over different guidance scales (each marked with a different color), and hyper-parameters α, γ, τ for ERG. Dashed lines trace the Pareto fronts for each plot. We measure consistency with VQAScore, quality with density and diversity with coverage.



Figure 3 Unconditional generation results. Compared to not using guidance, our ERG generates more realistic and detailed images and more coherent structure. Images obtained from T2I model at 512 with empty prompt inputs.

when compared to CFG). Additionally, ERG combined with APG achieves the overall best FID, recall and coverage, and second-best overall precision and density. Notably, our approach requires only two function evaluations (NFE) per inference step, which is comparable to other methods except SEG which requires three. These results suggest that our ERG approach is successfully able to boost the generation quality of the model in all three facets of generation (quality, diversity, and consistency).

Following Astolfi et al. (2024), we plot Pareto fronts for quality (measured by density), diversity (Coverage), and consistency (VQAScore) metrics in Figure 2 when using ERG + APG. We find all the points belonging to the Pareto fronts correspond to ERG + APG with APG. ERG + APG is able to improve all three facets of the generations w.r.t. APG, and provides significant boosts for quality and consistency. This can also be observed in the qualitative examples in Figure 1, where images sampled using our method show better visual quality than the baseline with classifier-free guidance.

| | FID | Precision | Recall | Density | Coverage |
|------------------------------------|--------------|--------------|--------------|--------------|--------------|
| No guidance | 101.50 | 13.50 | 38.22 | 8.99 | 3.63 |
| SAG (Hong et al., 2023) | 39.25 | 43.45 | 55.00 | 46.22 | 30.70 |
| PAG* (Ahn et al., 2024) | 41.50 | 42.91 | 62.86 | 45.65 | 30.51 |
| SEG* (Hong, 2024) | 37.75 | 48.99 | 50.10 | 55.56 | 34.79 |
| AutoGuidance (Karras et al., 2024) | 39.50 | 49.97 | 42.09 | 48.26 | 34.71 |
| ERG (ours) | 36.25 | 68.87 | 57.15 | 55.84 | 51.59 |

Table 2 Unconditional generation. Comparing no guidance, SEG, and I-ERG sampling from the text-to-image model.

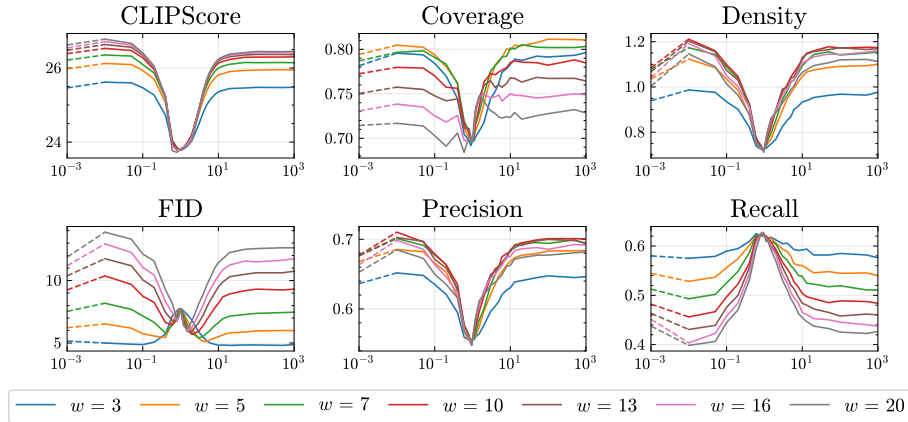


Figure 4 Temperature rescaling in the conditioning (C-ERG) for text-to-image generation. We vary the attention temperatures τ_c on the text encoder. Each curve represents one setting of the guidance strength w . The left-most point on each curve represents the result for standard CFG with the at weight.

| | Res. | FID | Precision | Recall | Density | Coverage |
|-----------------------------|------|-------------|--------------|--------------|---------------|--------------|
| CFG (Ho and Salimans, 2021) | | 3.67 | 76.63 | 55.70 | 127.03 | 85.81 |
| PAG* (Ahn et al., 2024) | | 5.31 | 72.38 | 52.55 | 111.94 | 81.04 |
| SAG (Hong et al., 2023) | 256 | 3.78 | 75.56 | 58.68 | 131.89 | 86.35 |
| SEG* (Hong, 2024) | | 6.15 | 77.97 | 48.10 | 132.22 | 84.51 |
| I-ERG (ours) | | 3.67 | 80.51 | 54.03 | 141.96 | 86.72 |
| CFG (Ho and Salimans, 2021) | | 5.65 | 81.39 | 49.06 | 146.97 | 86.70 |
| PAG* (Ahn et al., 2024) | | 4.65 | 78.04 | 52.44 | 134.49 | 86.50 |
| SAG (Hong et al., 2023) | 512 | 4.81 | 74.90 | 52.84 | 120.09 | 83.91 |
| SEG* (Hong, 2024) | | 6.59 | 82.88 | 33.25 | 160.11 | 81.85 |
| I-ERG (ours) | | 4.56 | 84.39 | 52.92 | 163.63 | 86.13 |

Table 3 Class-conditional generation. Comparison of ERG with other guidance methods for models trained for 256 and 512 resolution generation.

Unconditional generation. In the unconditional model sampling experiment, we compare our Entropy Rectifying Guidance with sampling without guidance and using applicable methods: AutoGuidance, SEG*, PAG* and SAG*. We provide quantitative evaluation results in Table 2. We find that ERG outperforms all other methods, except for Recall which is higher for the PAG* method (62.86 vs. 57.15 for ERG), with significant boosts in FID, precision, and coverage over other methods. The qualitative examples in Figure 3 clearly show artifacts in terms of structural coherence in all the objects present in the generated images when not using guidance, which disappear when using ERG.

Class-conditional generation. For class-conditional generation, we observe similar trends as the text-to-image setup in Table 3. Mainly, ERG boosts quality related metrics while maintaining similar performance in terms of diversity metrics (Recall and Coverage). At 256 resolution, we find large improvements in density, and smaller improvements in coverage and precision. FID remains similar to CFG but is better compared to all other methods tested. At 512 resolution, ERG is best across all metrics, except for coverage where ERG is slightly behind CFG and SEG*.

4.3 Analysis and ablations

Text Attention Energy. To isolate the effect of the temperature re-scaling in the conditioning, we experiment with C-ERG and disable temperature rescaling in the image denoising model. In Figure 4, we vary the SoftMax temperature τ_c used in the text encoder, and consider generation performance for different guidance strengths ω . For all metrics we find a somewhat symmetrical behavior around $\tau_c = 1$, which corresponds to an unguided prediction because in this case there is no difference with the normal conditional prediction. The CLIPScore, coverage, density, and precision metrics generally improve when moving away from $\tau_c = 1$, making it either larger or smaller, yet the reverse is seen for the recall metric. For FID the best values are obtained for intermediate temperature values for any setting of the guidance weight ω . While lower temperatures yield the best CLIPScore, higher temperatures are best for coverage and FID. Compared with standard classifier-free guidance (left-hand side of the dashed lines), we find that all metrics can be improved for any guidance scale, provided with the right temperature.

Table 4 Multi-step gradient descent for optimizing the energy landscape. The baseline corresponds to $K = 1, \tau = 1$.

| K | 1 | 1 | 10 |
|--------------------|--------|--------|---------|
| γ | 1.5 | 0.5 | 0.1 |
| Δ FID | 0.0 | +0.56 | +0.94 |
| Δ Precision | +1.02 | +1.44 | +5.37 |
| Δ Recall | +0.36 | -1.8 | -0.02 |
| Δ Density | +3.4 | +1.7 | -2.88 |
| Δ Coverage | +0.86 | -0.58 | -1.1 |
| Δ CLIP | -0.053 | -0.068 | -0.09 |
| Δ VQA | +0.71 | -0.95 | -0.0058 |

Table 5 Impact of the different components of ERG. We successively add different components of ERG, mainly C-ERG through conditioner entropy rectification, then I-ERG through denoiser entropy rectification and objective reweighting, finally all components are merged into ERG.

| Conditioner Entropy τ_c | \times | \checkmark | \checkmark | \checkmark |
|------------------------------|----------|--------------|--------------|---------------|
| Denoiser Entropy τ_i | \times | \times | \checkmark | \checkmark |
| Energy Reweighting α | \times | \times | \times | \checkmark |
| Density | 98.24 | 109.52 | 120.25 | 123.65 |
| Coverage | 71.12 | 72.06 | 73.21 | 74.07 |
| CLIPScore | 26.45 | 26.73 | 26.86 | 26.81 |

Combining the different parts. In Table 5, we combine different parts of the Entropy Rectifying Guidance and measure the effects on different facets of image generation. Our results show that all components show positive effects on the different facets of generation. Most of the improvement in CLIPScore are brought by the conditional entropy rectification (C-ERG, second column), while the improvements in Coverage and Density mostly come from modifying the image denoiser to obtain ERG (last column).

Multistep gradient descent. In Table 4 we the effect of varying the step-size γ and number of updates K for each attention operation. We find small variations in metrics with respect to the baseline $K = 1, \gamma = 1$ with slight positive variations when setting $\gamma = 1.5$, using multiple gradient descent steps did not induce significant gains in our case. Therefore, we used $K = 1, \gamma = 1$ in our default setup in our experiments, unless specified otherwise.

5 Conclusion

We presented a novel guidance mechanism for sampling diffusion and flow models – *Entropy Rectifying Guidance (ERG)* – which significantly improves quality without sacrificing diversity and consistency performance. In particular, by manipulating the energy landscape of the attention layers in the diffusion transformer and the text encoder at inference time, ERG significantly boosts the performance of the different models when studying their quality-consistency-diversity trade-offs and is applicable to different modalities such as text-to-image, class conditional and unconditional models. Furthermore, ERG outperforms different baselines such as CADs, APG, SEG and AutoGuidance while requiring the same compute as standard classifier-free guidance. ERG can be seamlessly combined with approaches such as APG and CADs in order to further improve sampling.

References

- Donghoon Ahn, Hyoungwon Cho, Jaewon Min, Wooseok Jang, Jungwoo Kim, SeonHwa Kim, Hyun Hee Park, Kyong Hwan Jin, and Seungryong Kim. Self-rectifying diffusion sampling with perturbed-attention guidance. In *European Conference on Computer Vision*, 2024. <https://arxiv.org/abs/2403.17377>.
- Pietro Astolfi, Marlene Careil, Melissa Hall, Oscar Mañas, Matthew Muckley, Jakob Verbeek, Adriana Romero Soriano, and Michal Drozdal. Consistency-diversity-realism Pareto fronts of conditional image generative models. *arXiv Preprint*, 2406.10429, 2024.
- Tariq Berrada, Pietro Astolfi, Melissa Hall, Reyhane Askari Hemmat, Yohann Benchetrit, Marton Havasi, Matthew J. Muckley, Karteek Alahari, Adriana Romero-Soriano, Jakob Verbeek, and Michal Drozdal. On improved conditioning mechanisms and pre-training strategies for diffusion models. In *Advances in Neural Information Processing Systems*, 2024. <https://openreview.net/forum?id=B3rZZRALhk>.
- Lucas Beyer, Andreas Steiner, André Susano Pinto, Alexander Kolesnikov, Xiao Wang, Daniel Salz, Maxim Neumann, Ibrahim Alabdulmohsin, Michael Tschannen, Emanuele Bugliarello, Thomas Unterthiner, Daniel Keysers, Skanda Koppula, Fangyu Liu, Adam Grycner, Alexey Gritsenko, Neil Houlsby, Manoj Kumar, Keran Rong, Julian Eisenschlos, Rishabh Kabra, Matthias Bauer, Matko Bošnjak, Xi Chen, Matthias Minderer, Paul Voigtlaender, Ioana Bica, Ivana Balazevic, Joan Puigcerver, Pinelopi Papalampidi, Olivier Henaff, Xi Xiong, Radu Soricut, Jeremiah Harmsen, and Xiaohua Zhai. Paligemma: A versatile 3b vlm for transfer, 2024. <https://arxiv.org/abs/2407.07726>.
- Junsong Chen, Jincheng Yu, Chongjian Ge, Lewei Yao, Enze Xie, Yue Wu, Zhongdao Wang, James Kwok, Ping Luo, Huchuan Lu, and Zhenguo Li. Pixart- α : Fast training of diffusion transformer for photorealistic text-to-image synthesis. In *International Conference on Learning Representations*, 2024.
- Hyung Won Chung, Le Hou, Shayne Longpre, Barret Zoph, Yi Tay, William Fedus, Yunxuan Li, Xuezhi Wang, Mostafa Dehghani, Siddhartha Brahma, Albert Webson, Shixiang Shane Gu, Zhuyun Dai, Mirac Suzgun, Xinyun Chen, Aakanksha Chowdhery, Alex Castro-Ros, Marie Pellat, Kevin Robinson, Dasha Valter, Sharan Narang, Gaurav Mishra, Adams Yu, Vincent Zhao, Yanping Huang, Andrew Dai, Hongkun Yu, Slav Petrov, Ed H. Chi, Jeff Dean, Jacob Devlin, Adam Roberts, Denny Zhou, Quoc V. Le, and Jason Wei. Scaling instruction-finetuned language models, 2022. <https://arxiv.org/abs/2210.11416>.
- J. Deng, W. Dong, R. Socher, L.-J. Li, K. Li, and L. Fei-Fei. ImageNet: A large-scale hierarchical image database. In *Conference on Computer Vision and Pattern Recognition*, 2009.
- Prafulla Dhariwal and Alex Nichol. Diffusion models beat GANs on image synthesis. In *Advances in Neural Information Processing Systems*, 2021.
- Patrick Esser, Sumith Kulal, Andreas Blattmann, Rahim Entezari, Jonas Müller, Harry Saini, Yam Levi, Dominik Lorenz, Axel Sauer, Frederic Boesel, Dustin Podell, Tim Dockhorn, Zion English, Kyle Lacey, Alex Goodwin, Yannik Marek, and Robin Rombach. Scaling rectified flow transformers for high-resolution image synthesis. In *International Conference on Machine Learning*, 2024.
- Aaron Grattafiori et al. The llama 3 herd of models, 2024. <https://arxiv.org/abs/2407.21783>.
- Melissa Hall, Oscar Mañas, Reyhane Askari, Mark Ibrahim, Candace Ross, Pietro Astolfi, Tariq Berrada Ifriqi, Marton Havasi, Yohann Benchetrit, Karen Ullrich, Carolina Braga, Abhishek Charnalia, Maeve Ryan, Mike Rabbat, Michal Drozdal, Jakob Verbeek, and Adriana Romero Soriano. Evalgim: A library for evaluating generative image models, 2024. <https://arxiv.org/abs/2412.10604>.
- Jack Hessel, Ari Holtzman, Maxwell Forbes, Ronan Le Bras, and Yejin Choi. CLIPScore: A reference-free evaluation metric for image captioning. In *Conference on Empirical Methods in Natural Language Processing*, 2021. <https://arxiv.org/abs/2104.08718>.
- Martin Heusel, Hubert Ramsauer, Thomas Unterthiner, Bernhard Nessler, and Sepp Hochreiter. GANs trained by a two time-scale update rule converge to a local Nash equilibrium. In *Advances in Neural Information Processing Systems*, 2017.
- Jonathan Ho and Tim Salimans. Classifier-free diffusion guidance. In *NeurIPS 2021 Workshop on Deep Generative Models and Downstream Applications*, 2021.
- Jonathan Ho, Ajay Jain, and Pieter Abbeel. Denoising diffusion probabilistic models. In *Advances in Neural Information Processing Systems*, 2020.

- Susung Hong. Smoothed energy guidance: Guiding diffusion models with reduced energy curvature of attention. In *Advances in Neural Information Processing Systems*, 2024. <https://arxiv.org/abs/2408.00760>.
- Susung Hong, Gyuseong Lee, Wooseok Jang, and Seungryong Kim. Improving sample quality of diffusion models using self-attention guidance. In *International Conference on Computer Vision*, 2023. <https://arxiv.org/abs/2210.00939>.
- J. J. Hopfield. Neural networks and physical systems with emergent collective computational abilities. *Proceedings of the National Academy of Sciences*, 79(8):2554–2558, 1982. doi: 10.1073/pnas.79.8.2554. <https://www.pnas.org/doi/abs/10.1073/pnas.79.8.2554>.
- Yang Jin, Zhicheng Sun, Ningyuan Li, Kun Xu, Kun Xu, Hao Jiang, Nan Zhuang, Quzhe Huang, Yang Song, Yadong Mu, and Zhouchen Lin. Pyramidal flow matching for efficient video generative modeling. In *International Conference on Learning Representations*, 2025. <https://arxiv.org/abs/2410.05954>.
- Tero Karras, Miika Aittala, Timo Aila, and Samuli Laine. Elucidating the design space of diffusion-based generative models. In S. Koyejo, S. Mohamed, A. Agarwal, D. Belgrave, K. Cho, and A. Oh, editors, *Advances in Neural Information Processing Systems*, volume 35, pages 26565–26577. Curran Associates, Inc., 2022. https://proceedings.neurips.cc/paper_files/paper/2022/file/a98846e9d9cc01cfb87eb694d946ce6b-Paper-Conference.pdf.
- Tero Karras, Miika Aittala, Tuomas Kynkäänniemi, Jaakko Lehtinen, Timo Aila, and Samuli Laine. Guiding a diffusion model with a bad version of itself. In *Advances in Neural Information Processing Systems*, 2024. <https://openreview.net/forum?id=bg6fVPVs3s>.
- Diederik P. Kingma and Ruiqi Gao. Understanding diffusion objectives as the ELBO with simple data augmentation. In *Advances in Neural Information Processing Systems*, 2023. <https://openreview.net/forum?id=NnMEadcdyD>.
- Tuomas Kynkäänniemi, Tero Karras, Samuli Laine, Jaakko Lehtinen, and Timo Aila. Improved precision and recall metric for assessing generative models. In *Advances in Neural Information Processing Systems*, 2019. <https://arxiv.org/abs/1904.06991>.
- Tuomas Kynkäänniemi, Miika Aittala, Tero Karras, Samuli Laine, Timo Aila, and Jaakko Lehtinen. Applying guidance in a limited interval improves sample and distribution quality in diffusion models. In *Advances in Neural Information Processing Systems*, 2024.
- Mark Levy, Bruno Di Giorgi, Floris Weers, Angelos Katharopoulos, and Tom Nickson. Controllable music production with diffusion models and guidance gradients. In *Advances in Neural Information Processing Systems*, 2023. <https://arxiv.org/abs/2311.00613>.
- Zhiqi Lin, Deepak Pathak, Baiqi Li, Jiayao Li, Xide Xia, Graham Neubig, Pengchuan Zhang, and Deva Ramanan. Evaluating text-to-visual generation with image-to-text generation, 2024. <https://arxiv.org/abs/2404.01291>.
- Yaron Lipman, Ricky T. Q. Chen, Heli Ben-Hamu, Maximilian Nickel, and Matthew Le. Flow matching for generative modeling. In *International Conference on Machine Learning*, 2023.
- Nanye Ma, Mark Goldstein, Michael S. Albergo, Nicholas M. Boffi, Eric Vanden-Eijnden, and Saining Xie. Sit: Exploring flow and diffusion-based generative models with scalable interpolant transformers, 2024. <https://arxiv.org/abs/2401.08740>.
- Muhammad Ferjad Naeem, Seong Joon Oh, Youngjung Uh, Yunjey Choi, and Jaejun Yoo. Reliable fidelity and diversity metrics for generative models. In *International Conference on Machine Learning*, 2020.
- Geon Yeong Park, Jeongsol Kim, Beomsu Kim, Sang Wan Lee, and Jong Chul Ye. Energy-based cross attention for Bayesian context update in text-to-image diffusion models. In *Advances in Neural Information Processing Systems*, 2024.
- Krunoslav Lehman Pavasovic, Jakob Verbeek, Giulio Biroli, and Marc Mezard. Understanding classifier-free guidance: High-dimensional theory and non-linear generalizations. *arXiv Preprint*, 2025.
- William Peebles and Saining Xie. Scalable diffusion models with transformers. In *International Conference on Computer Vision*, 2023.
- Dustin Podell, Zion English, Kyle Lacey, Andreas Blattmann, Tim Dockhorn, Jonas Müller, Joe Penna, and Robin Rombach. SDXL: Improving latent diffusion models for high-resolution image synthesis. In *International Conference on Learning Representations*, 2024.
- Adam Polyak, Amit Zohar, Andrew Brown, Andros Tjandra, Animesh Sinha, Ann Lee, Apoorv Vyas, Bowen Shi, Chih-Yao Ma, Ching-Yao Chuang, David Yan, Dhruv Choudhary, DingKang Wang, Geet Sethi, Guan Pang, Haoyu Ma, Ishan Misra, Ji Hou, Jialiang Wang, Kiran Jagadeesh, Kunkun Li, Luxin Zhang, Mannat Singh, Mary

- Williamson, Matt Le, Matthew Yu, Mitesh Kumar Singh, Peizhao Zhang, Peter Vajda, Quentin Duval, Rohit Girdhar, Roshan Sumbaly, Sai Saketh Rambhatla, Sam Tsai, Samaneh Azadi, Samyak Datta, Sanyuan Chen, Sean Bell, Sharadh Ramaswamy, Shelly Sheynin, Siddharth Bhattacharya, Simran Motwani, Tao Xu, Tianhe Li, Tingbo Hou, Wei-Ning Hsu, Xi Yin, Xiaoliang Dai, Yaniv Taigman, Yaqiao Luo, Yen-Cheng Liu, Yi-Chiao Wu, Yue Zhao, Yuval Kirstain, Zecheng He, Zijian He, Albert Pumarola, Ali Thabet, Artsiom Sanakoyeu, Arun Mallya, Baishan Guo, Boris Araya, Breena Kerr, Carleigh Wood, Ce Liu, Cen Peng, Dimitry Vengertsev, Edgar Schonfeld, Elliot Blanchard, Felix Juefei-Xu, Fraylie Nord, Jeff Liang, John Hoffman, Jonas Kohler, Kaolin Fire, Karthik Sivakumar, Lawrence Chen, Licheng Yu, Luya Gao, Markos Georgopoulos, Rashel Moritz, Sara K. Sampson, Shikai Li, Simone Parmeggiani, Steve Fine, Tara Fowler, Vladan Petrovic, and Yuming Du. Movie gen: A cast of media foundation models. *arXiv Preprint*, 2410.13720, 2024. <https://arxiv.org/abs/2410.13720>.
- Hubert Ramsauer, Bernhard Schöfl, Johannes Lehner, Philipp Seidl, Michael Widrich, Lukas Gruber, Markus Holzleitner, Milena Pavlovic, Geir Kjetil Sandve, Victor Greiff, David P. Kreil, Michael Kopp, Günter Klambauer, Johannes Brandstetter, and Sepp Hochreiter. Hopfield networks is all you need. In *International Conference on Learning Representations*, 2021. <https://arxiv.org/abs/2008.02217>.
- Robin Rombach, Andreas Blattmann, Dominik Lorenz, Patrick Esser, and Björn Ommer. High-resolution image synthesis with latent diffusion models. In *Conference on Computer Vision and Pattern Recognition*, 2022.
- Seyedmorteza Sadat, Jakob Buhmann, Derek Bradley, Otmar Hilliges, and Romann M. Weber. CADs: Unleashing the diversity of diffusion models through condition-annealed sampling. In *International Conference on Learning Representations*, 2024.
- Seyedmorteza Sadat, Otmar Hilliges, and Romann M. Weber. Eliminating oversaturation and artifacts of high guidance scales in diffusion models. In *International Conference on Learning Representations*, 2025. <https://arxiv.org/abs/2410.02416>.
- Chitwan Saharia, William Chan, Saurabh Saxena, Lala Li, Jay Whang, Emily L Denton, Kamyar Ghasemipour, Raphael Gontijo Lopes, Burcu Karagol Ayan, Tim Salimans, Jonathan Ho, David J Fleet, and Mohammad Norouzi. Photorealistic text-to-image diffusion models with deep language understanding. In S. Koyejo, S. Mohamed, A. Agarwal, D. Belgrave, K. Cho, and A. Oh, editors, *Advances in Neural Information Processing Systems*, 2022. https://proceedings.neurips.cc/paper_files/paper/2022/file/ec795aeadae0b7d230fa35cbaf04c041-Paper-Conference.pdf.
- Jascha Sohl-Dickstein, Eric Weiss, Niru Maheswaranathan, and Surya Ganguli. Deep unsupervised learning using nonequilibrium thermodynamics. In *International Conference on Machine Learning*, 2015. <https://proceedings.mlr.press/v37/sohl-dickstein15.html>.
- Yang Song, Jascha Sohl-Dickstein, Diederik P Kingma, Abhishek Kumar, Stefano Ermon, and Ben Poole. Score-based generative modeling through stochastic differential equations. In *International Conference on Learning Representations*, 2021. <https://openreview.net/forum?id=PXTIG12RRHS>.
- Xi Wang, Nicolas Dufour, Nefeli Andreou, Marie-Paule Cani, Victoria Fernandez Abrevaya, David Picard, and Vicky Kalogeiton. Analysis of classifier-free guidance weight schedulers. *Transactions on Machine Learning Research*, 2024. ISSN 2835-8856. <https://openreview.net/forum?id=SUMtDJqcd>.
- Yuancheng Wang, Zeqian Ju, Xu Tan, Lei He, Zhizheng Wu, Jiang Bian, and sheng zhao. Audit: Audio editing by following instructions with latent diffusion models. In *Advances in Neural Information Processing Systems*, 2023. https://proceedings.neurips.cc/paper_files/paper/2023/file/e1b619a9e241606a23eb21767f16cf81-Paper-Conference.pdf.
- Bin Xiao, Haiping Wu, Weijian Xu, Xiyang Dai, Houdong Hu, Yumao Lu, Michael Zeng, Ce Liu, and Lu Yuan. Florence-2: Advancing a unified representation for a variety of vision tasks. In *Conference on Computer Vision and Pattern Recognition*, 2024. <https://arxiv.org/abs/2311.06242>.
- A. Yuille and Anand Rangarajan. The concave-convex procedure. *Neural Computation*, 15:915–936, 04 2003. doi: 10.1162/08997660360581958.
- Zixin Zhu, Xuelu Feng, Dongdong Chen, Jianmin Bao, Le Wang, Yinpeng Chen, Lu Yuan, and Gang Hua. Designing a better asymmetric VQGAN for StableDiffusion. *arXiv Preprint*, 2306.04632, 2023.

A Definitions and Background

Background on Diffusion. Consider a data point \mathbf{x} drawn from the distribution $p_{data}(x)$, and let t be a time step within the interval $[0, 1]$. The forward process is defined as $\mathbf{x}_t = \mathbf{x} + \sigma(t)\boldsymbol{\epsilon}$, where Gaussian noise $\boldsymbol{\epsilon} \sim \mathcal{N}(0, \mathbf{I})$ is added to the data. The function $\sigma(t)$ is monotonically increasing, with boundary conditions $\sigma(0) = 0$ and $\sigma(1) = \sigma_{\max}$, where σ_{\max} is significantly larger than σ_{data} . Karras et al. (2022) demonstrated that the progression of the noisy samples \mathbf{x}_t can be captured by an ordinary differential equation (ODE):

$$d\mathbf{x} = -\dot{\sigma}(t)\sigma(t)\nabla_{\mathbf{x}_t} \log p_t(\mathbf{x}_t)dt \quad (11)$$

Alternatively, this can be expressed as a stochastic differential equation (SDE):

$$d\mathbf{x} = -\dot{\sigma}(t)\sigma(t)\nabla_{\mathbf{x}_t} \log p_t(\mathbf{x}_t)dt - \beta(t)\sigma(t)^2\nabla_{\mathbf{x}_t} \log p_t(\mathbf{x}_t) + \sqrt{2\beta(t)\sigma(t)}d\boldsymbol{\omega}_t \quad (12)$$

In this context, $d\boldsymbol{\omega}_t$ represents the standard Wiener process, and $p_t(\mathbf{x}_t)$ denotes the distribution of the perturbed samples, with initial and final conditions $p_0 = p_{data}$ and $p_1 = \mathcal{N}(0, \sigma_{max}^2 \mathbf{I})$, respectively.

To sample from diffusion models, one must solve the diffusion ODE or SDE in reverse, moving from $t = 1$ back to $t = 0$. This process relies on the time-dependent score function $\nabla_{\mathbf{x}_t} \log p_t(\mathbf{x}_t)$, which is approximated by a denoiser $v_\theta(\mathbf{x}_t, t)$. This denoiser is trained to predict the original clean samples \mathbf{x} from their noisy counterparts \mathbf{x}_t .

The framework also supports conditional generation by employing a denoiser $v_\theta(\mathbf{x}, t, y)$ that incorporates additional input signals y , such as class labels or textual prompts, allowing for more controlled and specific sample generation.

Latent Diffusion Models (LDMs). Are a class of generative models, proposed by Rombach et al. (2022), that operate in a latent space induced by a pretrained and frozen autoencoder. The autoencoder converts all images into latents of smaller resolution, inducing a space in which the generative model is trained, afterwards the latents can be converted back into image space by using the decoder of the autoencoder.

A.1 Rank Scoring

As different guidance methods require their own set of hyperparameters, and may respond differently to shared hyperparameters, we select the best hyperparameter set for each method using a global score. The global score is computed as the average ranking across all tracked metrics, where the ranking is determined within the pool of tested hyperparameter combinations.

B Additional Experiments

B.1 C-ERG Impact on diversity

To better understand the effect of c-ERG on diversity, we perform a simple experiment where we track the initial velocity direction during sampling and how it varies when the initial noised input $\mathbf{x}_0 = \boldsymbol{\epsilon} \sim \mathcal{N}(0, \mathbf{I})$ varies.

We examine the variance of the predicted velocity at the start of sampling, conditioning either on the encoding of an empty prompt $\boldsymbol{\phi}_\emptyset$ or on the encoding of caption using temperature rescaled attention layers $\boldsymbol{\phi}_c^r$. For this we sample $N = 20$ random noise inputs and compare the variance when the inputs vary, the right panel of Figure 5 presents a histogram of the variances where each datapoint corresponds to different spatial/channel location; we refer to it this as *marginal* variance:

$$\left\{ \begin{array}{l} \text{Var}_{\substack{\boldsymbol{\epsilon} \sim \mathcal{N}(0, \mathbf{I}) \\ c \sim D_c}} [v_\Theta(\boldsymbol{\epsilon}, \boldsymbol{\phi}_\emptyset, t = 0)], \\ \text{Var}_{\substack{\boldsymbol{\epsilon} \sim \mathcal{N}(0, \mathbf{I}) \\ c \sim D_c}} [v_\Theta(\boldsymbol{\epsilon}, \boldsymbol{\phi}_c^r, t = 0)]. \end{array} \right. \quad (13)$$

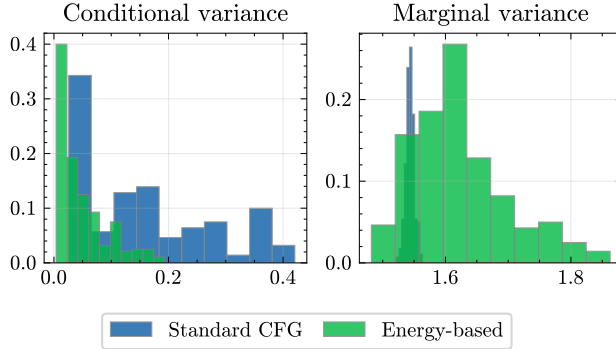


Figure 5 Effect of C-ERG on initial velocity step. Standard CFG shows very localized initial marginal variance while the conditional variance is much larger. This means that the negative model predicts an initial velocity that is very similar when varying the initial noise (and prompt in case of C-ERG), and is largely decorrelated from the conditional prediction, leading to a lack of diversity in the generated samples. Conversely, C-ERG results in much higher marginal variance and smaller conditional variance, reducing the error accumulation that can happen at earlier timesteps and leading to better diversity.

where D_c is a dataset of text prompts.

Similarly, in the right panel of Figure 5 we consider the variance of the difference between these velocity estimates and the true conditional one, i.e. when we condition on ϕ_c ; we refer to this as *conditional* variance:

$$\begin{cases} \text{Var}_{\epsilon \sim \mathcal{N}(0, I)} [v_{\Theta}(\epsilon, \phi_c, t = 0) - v_{\Theta}(\epsilon, \phi_{\emptyset}, t = 0)], \\ \text{Var}_{\epsilon \sim \mathcal{N}(0, I)} [v_{\Theta}(\epsilon, \phi_c, t = 0) - v_{\Theta}(\epsilon, \phi_c^{\tau}, t = 0)]. \end{cases} \quad (14)$$

From Figure 5, we observe that standard classifier-free guidance results in a larger range for the conditional variance while the marginal variance is significantly reduced. In contrast, C-ERG exhibits a larger range of marginal variances but a smaller range of conditional variances. Such results indicate that standard classifier-free guidance with high guidance scales operate as an initial condition for the flow ODE (equation (11)) that has low variance, resulting in exploring only a subset of the solutions of the ODE. Furthermore, as the initial conditional velocity is much larger, it can easily cause overshooting problems as large updates are being taken with a flawed prediction because of imperfections in the model, while the low marginal variance results in oversaturated colors and simplified image compositions. Similar observations were made by Saharia et al. (2022); Kynkäänniemi et al. (2024); Sadat et al. (2025).

Qualitative results corroborate this, see for example Figure 1 where using standard CFG results in low diversity, saturated images with simple compositions, while our ERG is able to generate more complex scenes that suffer less from the “cartoonish” effect, especially for highly out-of-distribution prompts where the denoiser model is expected to be less accurate.

B.2 I-ERG Impact on quality

To better understand the differences between I-ERG and CFG, we consider the difference between the two denoising terms used in CFG and I-ERG, see Equation (14). In particular we decompose the difference into parallel and orthogonal components to the conditional prediction, and track the magnitude of these components throughout the sampling process.

Results in Appendix B.2 reveal a fundamental difference between I-ERG and CFG. The parallel differences show similar trends between CFG and I-ERG: a peak around $t = 0.075$ followed by a sharp decline towards zero, indicating that for approximately $t \geq 0.4$ the denoising task becomes easy enough that both conditional and unconditional predictions yield similar and correlated results. On the other hand, when examining the orthogonal component of the differences, we see that it keeps a steady norm through sampling while in the case of standard CFG, the norm of the orthogonal difference quickly decreases as sampling progresses for

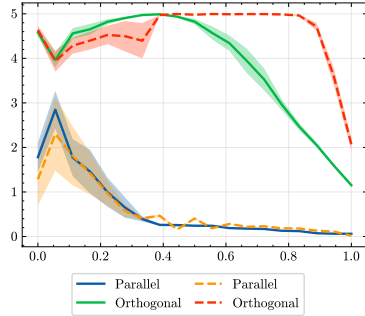


Figure 6 Orthogonal and parallel differences during sampling. Solid lines correspond to the parallel and orthogonal differences between the conditional and unconditional prediction of the model under standard CFG while dashed lines correspond to those of I-ERG. The sampling process proceeds from left ($t = 0$) to right ($t = 1$) over the horizontal axis.

Table 6 Comparison between different mechanisms for attention rectification. Conducted when using I-ERG.

| | FID (\downarrow) | Precision (\uparrow) | Recall (\uparrow) | Density (\uparrow) | Coverage (\uparrow) | CLIPScore (\uparrow) |
|-------------------------------------|----------------------|--------------------------|-----------------------|------------------------|-------------------------|--------------------------|
| Energy Smoothing $\sigma = +\infty$ | 15.06 | 66.39 | 39.24 | 102.82 | 69.45 | 26.60 |
| Identity mapping | 16.62 | 69.40 | 35.37 | 111.83 | 70.76 | 26.42 |
| Temperature reduction | 14.43 | 69.95 | 36.57 | 114.50 | 71.44 | 26.71 |

$t \geq 0.4$, this indicates strong correlations between conditional and unconditional predictions as the denoising task becomes easier and the denoiser needs less to rely on the conditional embeddings.

While [Sadat et al. \(2025\)](#) completely eliminate the parallel component from the difference term, we are able to break such correlations by manipulating the energy landscape of the attention layers of the denoiser. Imposing this divergence between the positive and negative predictors results in semantically meaningful errors for the negative velocity prediction which, when used as a guidance term, improves the low-level details in the resulting image.

Notice that the I-ERG kickoff threshold κ corresponds to the point where the parallel difference between the predicted velocities converges towards 0 while the orthogonal part starts decreasing in a quasi-linear manner, this indicates that the optimal value for κ can be obtained with a simple analysis of the correlation between positive/conditional and negative/unconditional predictions of the model.

B.3 Attention rectification mechanisms

In [Table 6](#), we compare different attention rectification mechanisms from the literature, including energy smoothing (from SEG) ([Hong, 2024](#)), identity mapping (from PAG) ([Ahn et al., 2024](#)) and temperature reduction at the denoiser level as is done in I-ERG. We use a guidance scale of 5.0 and $\tau = 0.2$. Our experiments indicate better performance when using low attention temperature when compared to both energy smoothing and identity mapping in the attention. The most notable difference being in density which is 12 points higher for temperature reduction compared to energy smoothing and 3 points higher than identity mapping. Similarly, temperature reduction achieves the best FID at 14.43 which is 0.6 points lower than energy smoothing and 2.2 points better than identity mapping. Compared to energy smoothing, Identity mapping, as proposed in [Ahn et al. \(2024\)](#), achieves better precision, density, coverage and CLIPScore than energy smoothing but still underperforms when compared to temperature reduction. Similar results can be observed qualitatively in [Figure 17](#), temperature reduction generates images that showcase better realism in terms of the details of the image such as wooden textures on the floor in the first row, and details on the musician’s face and the background in the second row. Similarly, other qualitative results provide evidence supporting this effect, for example in [Figure 12](#) and [Figure 18](#) we observe more detailed backgrounds when using I-ERG than SEG.

B.4 Attention Blocks

In order to uncover the role of different attention blocks on the sampling process, we track the number of tokens where the maximum probability in the (non-rectified) attention is superior to a threshold of 0.95, resulting in a near one-to-one matching between the predicted queries and values.

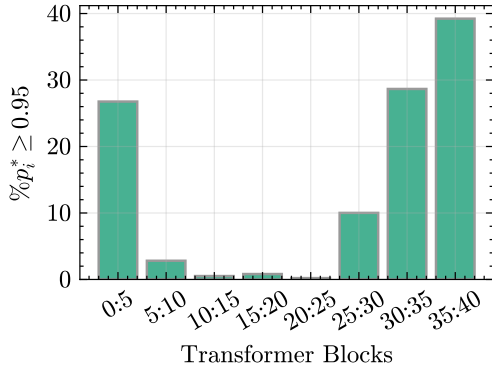


Figure 7 Percentage of points in the attention matrix that have a high maximum probability. We observe three different regimes depending on the depth of the block. For blocks [0-5], the maximal association probability is high with more than 25% of tokens having a maximum probability superior to 0.95, For blocks 0-25, the association probability is rarely above 95%. Finally, the proportion of high certainty associations grows back for deeper layers in the model [25-38], reaching almost 40% for the last layers 35 – 38.

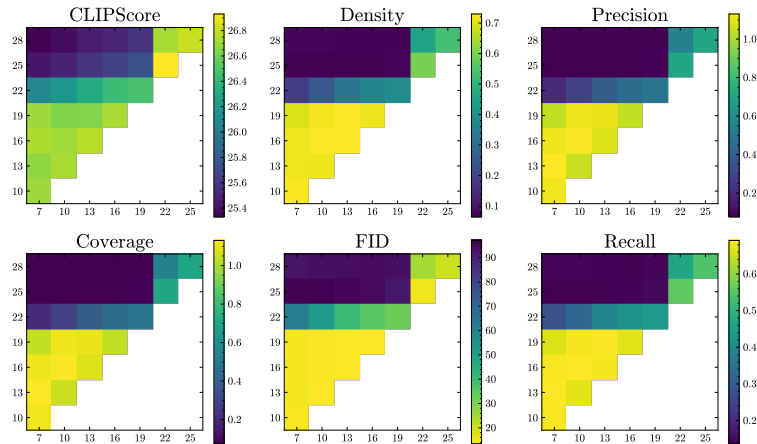


Figure 8 Choice of Rectified Attention Layers. Impact of the attention layers where the energy landscape is modified for I-ERG. (x-axis: start block, y-axis: end block). Operating ERG on middle layers seems to favorably impact performance, while including later layers results in harmful effects.

Our results (for $t = 0.3$) are summarized in Figure 7. We find a similar pattern across the different sampling steps. We observe three different regimes through the different layers of the model. While the first and last stage have a reasonably high matching probability, the middle stage has much smaller maximum probabilities and thus combines information from multiple tokens.

With this in mind, we posit that the energy landscape manipulations should only happen in the middle regime, as it would not overly harm the representations of the model. To validate this intuition, we perform a grid search over the range of blocks in which the energy manipulation is performed, we find a similar trend with the emergence of three different regimes, we find the best performance when applying the energy guidance on the middle blocks.

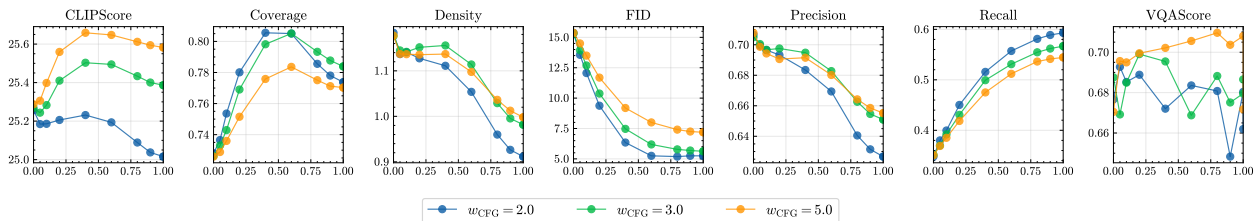


Figure 9 Influence of I-ERG kickoff threshold κ . Experiment conducted on our T2I model using Euler sampler with 50 steps. We observe different trends for different metrics, FID and Recall are improved as κ goes to 1, precision and density on the other hand are improved when κ goes to 0, CLIPScore, VQAScore and coverage are optimal for κ in the middle of the range $\kappa \in [0.2, 0.6]$.

| Task | Text encoder | κ | l_{\min}^i | l_{\max}^i | τ_i | l_{\min}^c | l_{\max}^c | τ_c | α | γ | K |
|--|----------------|----------|--------------|--------------|----------|--------------|--------------|--------------|----------|----------|-----|
| <i>Text-to-image (MMDiT-B/2)</i> | llama3 T5 | 0.4 | 10 | 17 | 0.01 | 0 0 | 32 24 | 0.01 0.01 | 1.0 | 1.5 | 1.0 |
| <i>Unconditional (from text2image) (MMDiT-B/2)</i> | — | 0.2 | 10 | 17 | 0.01 | — | — | — | 1.0 | 1.0 | 1.0 |
| <i>Class-conditional (DiT-XL/2)</i> | — | 0.3 | 12 | 15 | 0.01 | — | — | — | 1.0 | 1.0 | 1.0 |
| <i>Text-to-image (SD3-medium)</i> | OpenCLIP-ViT/G | | | | | 1 | 31 | 0.1 | | | |
| | CLIP-ViT/L | 0.2 | 6 | 8 | 0.01 | 1 | 10 | 0.1 | 1.0 | 1.0 | 1.0 |
| | T5-xxl | | | | | 1 | 22 | 0.1 | | | |

Table 7 Sampling parameters for different settings. We provide the default hyperparameters used in our experiments grouped by model and modality.

B.5 I-ERG kickoff threshold

In [Figure 9](#), we perform a sweep over the kickoff threshold κ for the denoiser-level energy guidance, with the temperature rescaling parameter set as $\tau_i = 0.01$.

For density and precision, we achieve uniform improvements as κ becomes smaller. For CLIPScore, coverage, and VQAScore, we observe better improvements when κ is shifted to the middle of the time range. For recall and FID, we observe consistent degradation as the range of timesteps in which denoiser energy guidance is applied gets larger.

As reported in [Astolfi et al. \(2024\)](#), there is a natural trade-off between different facets of the generation *i.e* quality, consistency and diversity. While lower thresholds achieve the best precision and density (*quality*), higher thresholds notably improve coverage, recall and FID (*diversity*). On the other hand, CLIPScore and VQA (consistency) are maximized for a mid level threshold. This indicates that κ can be tuned according to the task at hand to achieve suitable results, we find in our experiments that setting $\kappa \in [0.2, 0.4]$ achieves the most balanced performance across different settings.

C Implementation

In this section, we provide pseudo-code in the style of pytorch to implement ERG.

I-ERG. Changing standard attention mechanism with the energy-based variant defined in [Algorithm 1](#) and applying this for attention blocks between l_{\min} and l_{\max} in the negative/unconditional prediction. Only applied if $t > \kappa$.

C-ERG. For the negative prediction, instead of having the prediction conditioned on empty text tokens, we condition it on tokens obtained by forwarding the text prompts through the text encoder while changing the temperature of the attention in the text encoders between layers l_{\min}^c and l_{\max}^c from β to $\beta \cdot \tau_c$. Applies for all timesteps.

ERG. Consists in applying both I-ERG and C-ERG.

In [Listing 1](#), we provide a function that applies the temperature rescaling in the attention layers of text-encoders by utilizing forward hooks on the query mapping. In practice, the temperature rescaling is equivalent to rescaling of the queries prior to the attention operation.

In [Listing 2](#), we provide code for the energy-based attention in the case of the mutli-modal transformer block used in [Esser et al. \(2024\)](#).

In [Table 7](#), we provide different hyperparameter sets used for our ERG method under different settings. We consider these values as the defaults used for our experiments unless specified otherwise.

```

def forward_with_temperature(transformer, prompts,
                             tau=0.01, l_min=15, l_max = 20):
    handles = []

    # define forward_hook_function.
    def hook(module, input, output):
        output[:] *= tau
        return output

    # register forward hooks.
    for i in range(l_min, l_max):
        handle = transformer.blocks[i].self_attn.q_proj.register_forward_hook(hook)
        handles.append(handle)

    # encode prompts.
    encoder_hidden_states = transformer.encode(prompts)

    # remove registered_hooks.
    for hook in handles:
        hook.remove()

    return encoder_hidden_states

```

Algorithm 1 Pseudo-code for temperature scaled encoding of prompts. Written using Pytorch functionalities.

| | FID | Precision | Recall | Density | Coverage | CLIPScore |
|-----|--------------|--------------|--------------|---------------|--------------|--------------|
| CFG | 35.85 | 40.09 | 43.17 | 41.11 | 10.95 | 24.71 |
| ERG | 25.82 | 68.59 | 38.66 | 114.67 | 24.29 | 27.71 |

Table 8 Effect of ERG on Stable Diffusion 3 model. We compare standard classifier-free guidance with our method on COCO-5K benchmark. We observe significant improvements across the different metrics.

D Combining different methods

ERG + APG. APG can be seamlessly integrated with ERG by switching the guidance update to the APG update, as both conditional and unconditional predictions can be converted into clean latent estimates, the algorithm operates as described by [Sadat et al. \(2025\)](#). In the case of rectified flows, such a conversion is easily obtained as $\hat{\mathbf{x}}_0 = \mathbf{x}_t + (1 - t) \cdot \hat{\mathbf{v}}_{\Theta}(\mathbf{x}_t, \phi, t)$. After the guidance update, the clean image estimate is projected back into velocity prediction by inverting the formula: $\hat{\mathbf{v}}_{\Theta}(\mathbf{x}_t, \phi, t) = (\hat{\mathbf{x}}_0 - \mathbf{x}_t)/(1 - t)$.

ERG + CADs. CADs is also straightforward to integrate with ERG, for this we switch the text encoder hidden states in the conditional/positive prediction with the interpolation between the tokens and Gaussian noise as described by [Sadat et al. \(2024\)](#).

E Reimplementation

We implement our method on the open-source stable diffusion 3 model, we use the `sd3-medium` from `diffusers` library. We refer to [Table 7](#) for details about the choice of hyperparameters, additional qualitative examples on [Figure 19](#) show significant improvements in terms of image quality. In [Table 8](#), we report quantitative results on this model on COCO-5K benchmark. For this experiment we use the standard setup with a guidance scale of 5.0 and Euler sampler with 28 steps. We observe significant improvements for all metrics other than recall when using ERG compared to standard classifier-free guidance. More precisely, we observe significant boosts in FID -10.03 pts, density $+73.56$, coverage $+13.34$ and CLIPScore $+3.0$.

F Additional qualitative results

We provide additional qualitative examples of our model under different settings.

In [Figure 10](#), we provide a comparison between classifier-free guidance and Entropy Rectifying Guidance on

```

def multistep_attention(q,k,v,step_size=1.0,steps=1, gamma=1.0):
    q_new = q.clone()
    for i in range(steps):
        att = scaled_dot_product_attention(q_new,k,v)
        q_new = q_new - step_size * (q_new - gamma * att)
    return q_new

def energy_based_attention(self, x, rope_freqs, num_img_tokens, tau_i):
    B, N, C = x.shape
    # B: batch size — N: Number of tokens — C: Hidden dimension.
    s1 = num_img_tokens

    q = self.q_linear(x).reshape(
        B, N, num_heads, C // num_heads
    ).permute(0, 2, 1, 3)
    kv = kv_linear(x).reshape(
        B, N, 2, num_heads, C // num_heads
    ).permute(2, 0, 3, 1, 4)

    k, v = kv.unbind(0)
    q = self.q_norm(q)
    k = self.k_norm(k)

    # Optionally apply rotary positional embeddings.
    qi, qc = q[:, :, :s1], q[:, :, s1:]
    ki, kc = k[:, :, :s1], k[:, :, s1:]
    qi, ki = apply_rotary_emb(qi, ki, rope_freqs=rope_freqs)

    # Entropy rectification in the image tokens.
    if tau_i > 0:
        qi[:, :] = qi[:, :] * tau_i

    q = torch.cat([qi, qc], dim=2)
    k = torch.cat([ki, kc], dim=2)

    if not self.use_e_att:
        x = scaled_dot_product_attention(q, k, v)
    else:
        x = multistep_attention(
            q,
            k,
            v,
            lr=self.step_size,
            steps=self.num_steps,
            gamma=self.potential_w,
        )

    x = x.transpose(1, 2).reshape(B, N, C)
    x = proj(x)
    return x

```

Algorithm 2 Pseudo-code for temperature scaled encoding of prompts. The hidden state \mathbf{x} consists of image tokens concatenated with text/class tokens.

three different prompts with varying levels of detail, we showcase the conditional diversity of the methods by providing samples with 5 different random seeds for each prompt. For longer prompts (top row), we observe similar consistency but higher diversity in terms of background colors, the dog’s physical traits etc. Similarly, second row shows increased diversity with LPL in terms of colors, textures and the drawing that the cat is holding. For very short prompts (third row), we observe certain redundancies in the standard CFG generations while LPL is able to generate high quality samples showcasing higher diversity (imagining the horse in different situations, different angles for the picture, different time of day etc).

In [Figure 11](#), we provide a comparison between classifier-free guidance and I-ERG showcasing the improvements in image quality when generating samples with the same random seed. By setting $\tau_i = 0.2$, the image semantics are not steered excessively compared to the CFG generations, resulting in comparable generations. We observe noticeable improvements in terms of high level details in the images when using I-ERG.

In [Figure 12](#), we provide comparisons between vanilla generation (no guidance), our implementations of SAG, PAG, SEG, and I-ERG for unconditional image generation. While PAG*, and SEG* are also able to improve image quality to satisfying levels, I-ERG provides an additional level of detail that is not present in the other methods (table texture on second row, background in the third and fifth row, water texture in fourth row and

grass texture in the fifth row.

In [Figure 13](#), we provide qualitative comparisons between different methods for text-to-image generation. We compare our method with CFG, CADs and APG. We also provide samples generated when combining our method with either APG or CADs. Each column corresponds to a unique random seed that is used for the generations. We observe that both CFG and CADs tend to generate images that have a cartoonish style, APG on the other hand generates images that are more realistic looking. ERG alone significantly boosts image realism and results in less saturated images (pure white/black backgrounds for example). Mixing, ERG with either CADs or APG results in significant improvements in both image quality and diversity.

In [Figure 14](#), we provide a qualitative comparison between APG and APG + ERG, similar to [Figure 1](#), we observe improvements in image quality and diversity. Also noticeable is a drift from unrealistic image styles (cartoonish) towards more realistic as can be seen in the astronaut and panda examples.

In [Figure 15](#), we showcase the effect of the image kickoff threshold κ and denoiser attention temperature τ_i by interpolating both parameters in an unconditional generation experiment. We observe that lowering the attention temperature $\tau_i \rightarrow 0$ results in improved image quality. Similarly, lowering the image kickoff threshold κ further improves image quality but steers the semantics of the image away from the vanilla generation ($\kappa = 1.0, \tau_i = 1$). However, as the image level threshold gets smaller $\kappa \rightarrow 0$, the semantics of the original image diverge from the vanilla generations, resulting in images with largely different semantics. We find $\kappa \in [0.2, 0.4]$ and $\tau_i = 0.01$ to work well in most cases.

In [Figure 16](#), we illustrate the effect of applying I-ERG on different layers of the denoiser. This experiment is conducted for class-conditional ImageNet-1K generations with our DiT-XL/2 model with 28 layers. We apply I-ERG to a different range of layers where three layers are involved each time. Applying I-ERG to either very early or late layers results in similar effects, with noticeable over-saturation and unnatural patterns that are overly simplistic as can be seen in the dog’s fur. On the other hand, applying I-ERG to middle layers results in improved image quality and sharper details. We find $l_{\min} = 12, l_{\max} = 15$ for the rest of the experiments to work well in this setup.

In [Figure 18](#), we provide qualitative results comparing I-ERG with SEG and CFG for class-conditional generation on ImageNet at 512 resolution, using a DiT-XL/2 model. Similarly to the unconditional and text-to-image cases, we find I-ERG to achieve higher image quality when compared CFG and our reimplementations of other guidance methods.

“A french bulldog wearing a red sweater and a blue hat, sitting at a table with a person’s hand holding a doughnut in front of it. The background of the image is a wall.”



“A small kitten holding a sign. The sign shows a fish drawing.”



“A horse.”

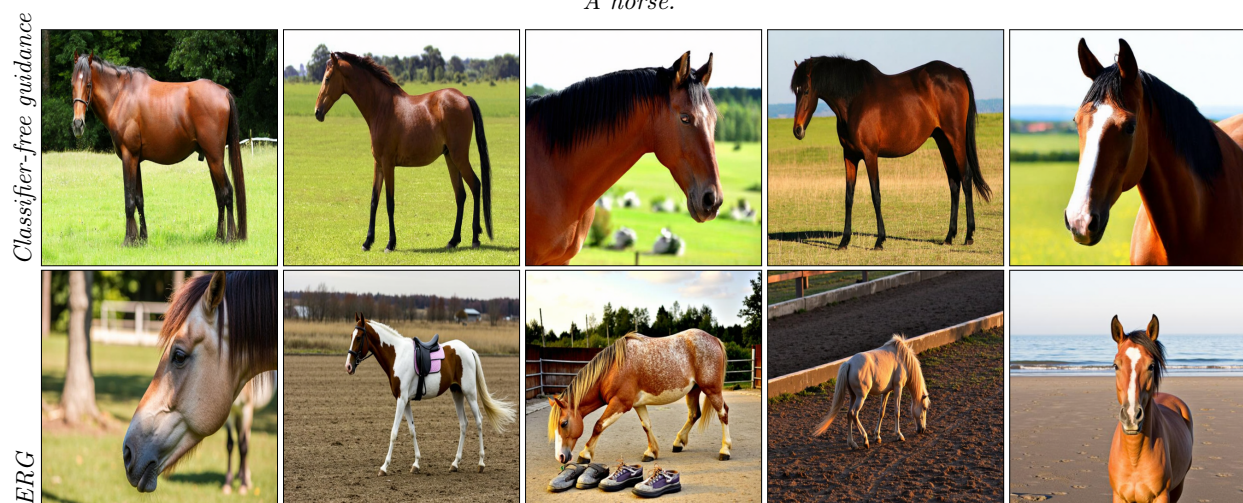


Figure 10 Qualitative comparison standard classifier-free guidance (top) and Entropy Rectifying Guidance (bottom). Each column represents images generated using the same random seed. Images generated with scaled temperature show more complex textures and variations than the standard guidance.

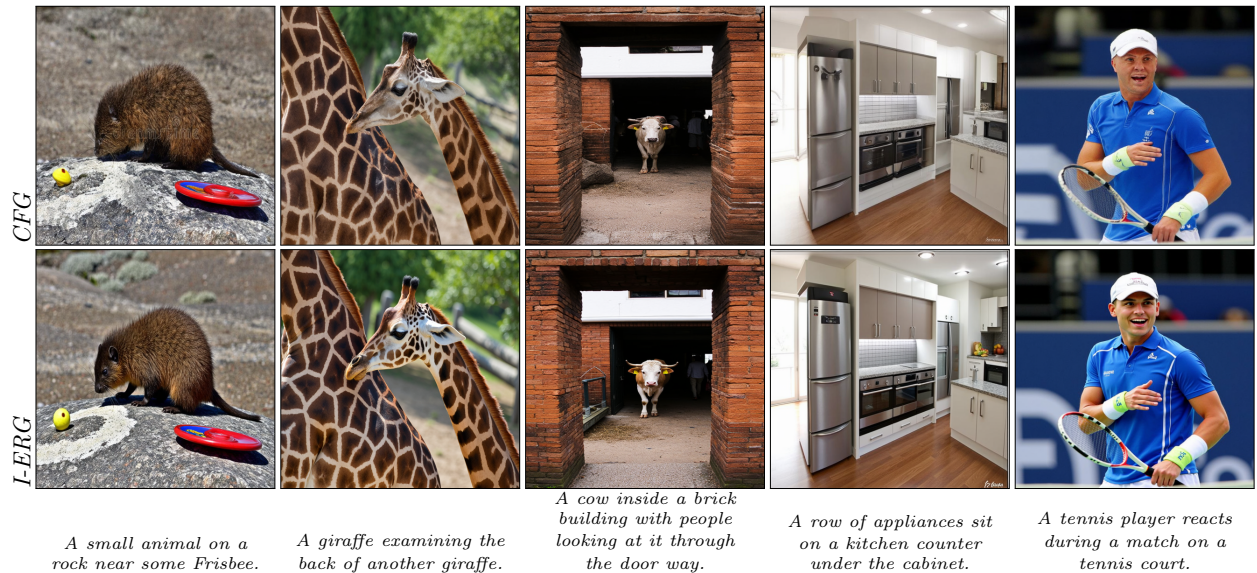


Figure 11 Influence of I-ERG on boosting image quality. Top row: images generated with standard guidance. Bottom row: images generated with $\alpha = 0.01$, a guidance scale of $w_{CFG} = 3.0$ and $\tau = 0.2$ order to match the image semantic in the comparison.

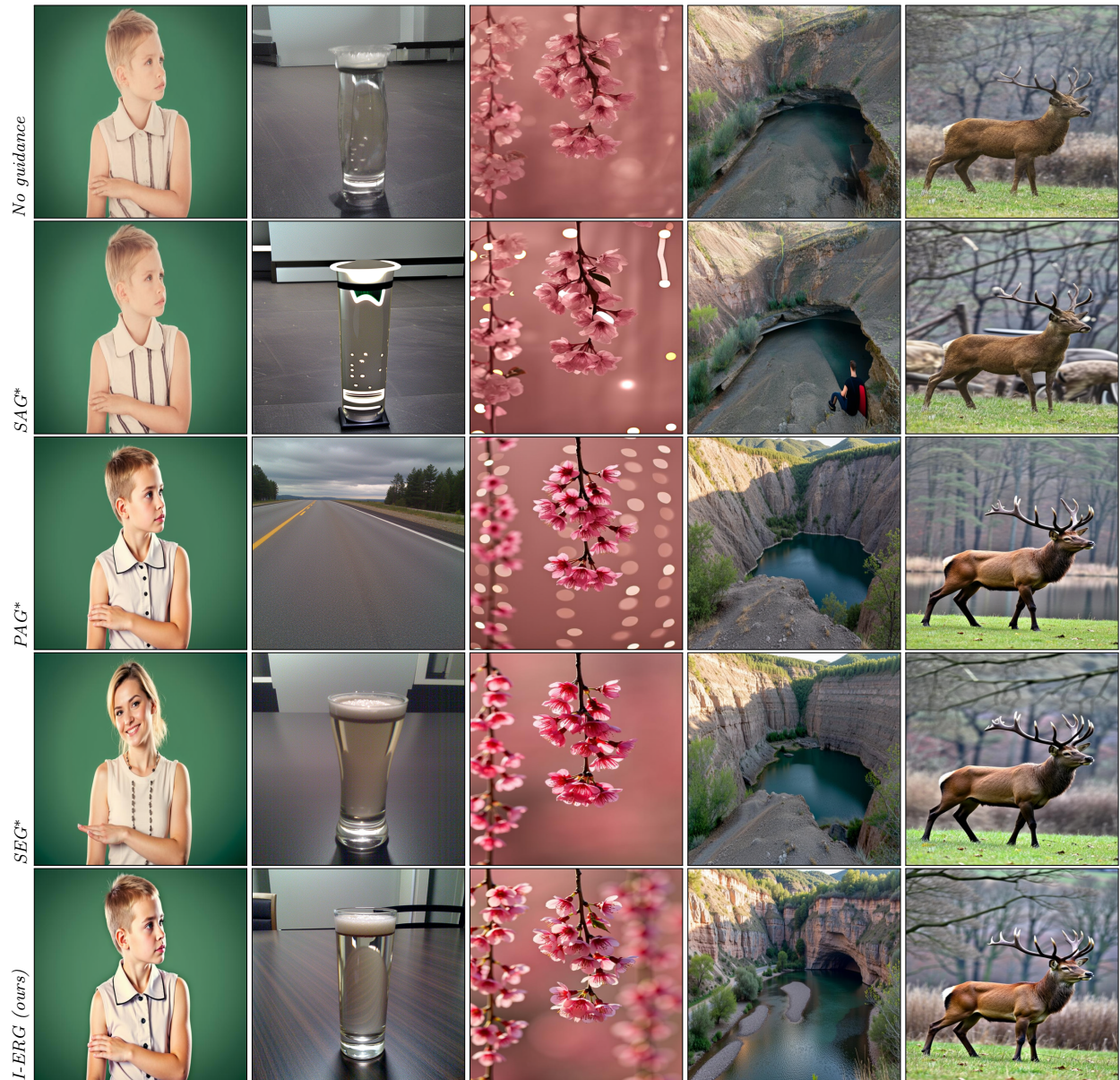


Figure 12 Comparing different methods for unconditional image generation. Images are sampled from the text-to-image model while conditioning on an empty prompt, using a guidance scale of 3.0 and Euler sampler with 50 sampling steps.

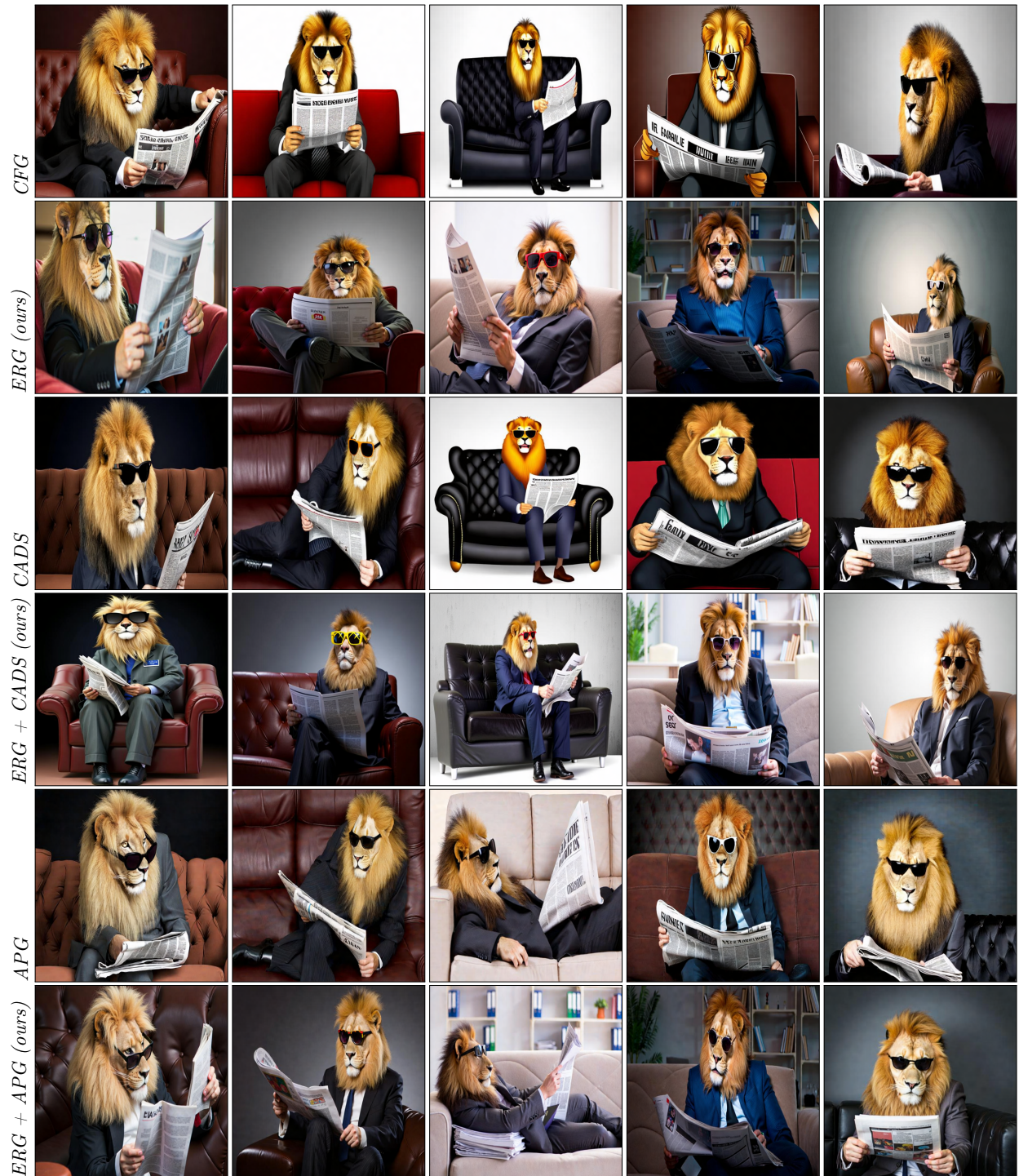


Figure 13 Qualitative comparison between different methods. We provide a detailed qualitative comparison between different methods, we use the “A lion with sunglasses and a suit, seated in a sofa, reading the newspaper.” and sample images with 5 different random seeds, each corresponding to a column in the figure.



Figure 14 Qualitative comparison showcasing the effect of Entropy Rectifying Guidance (ERG) on generation quality when combined APG.



Figure 15 Effect of I-ERG main parameters. Interpolating the image kickoff threshold κ on the vertical axis and denoiser attention temperature τ_i on the horizontal axis, we can see the effect on image quality. Unconditional generation experiment, $w_{CFG} = 3.0$.

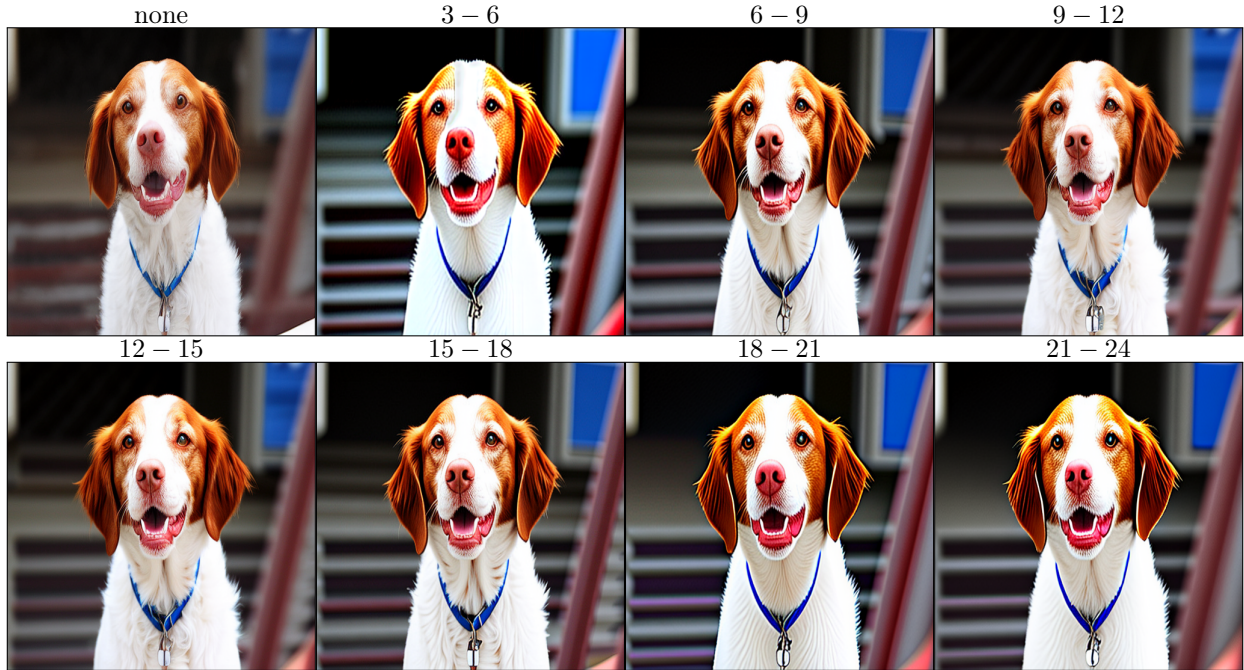
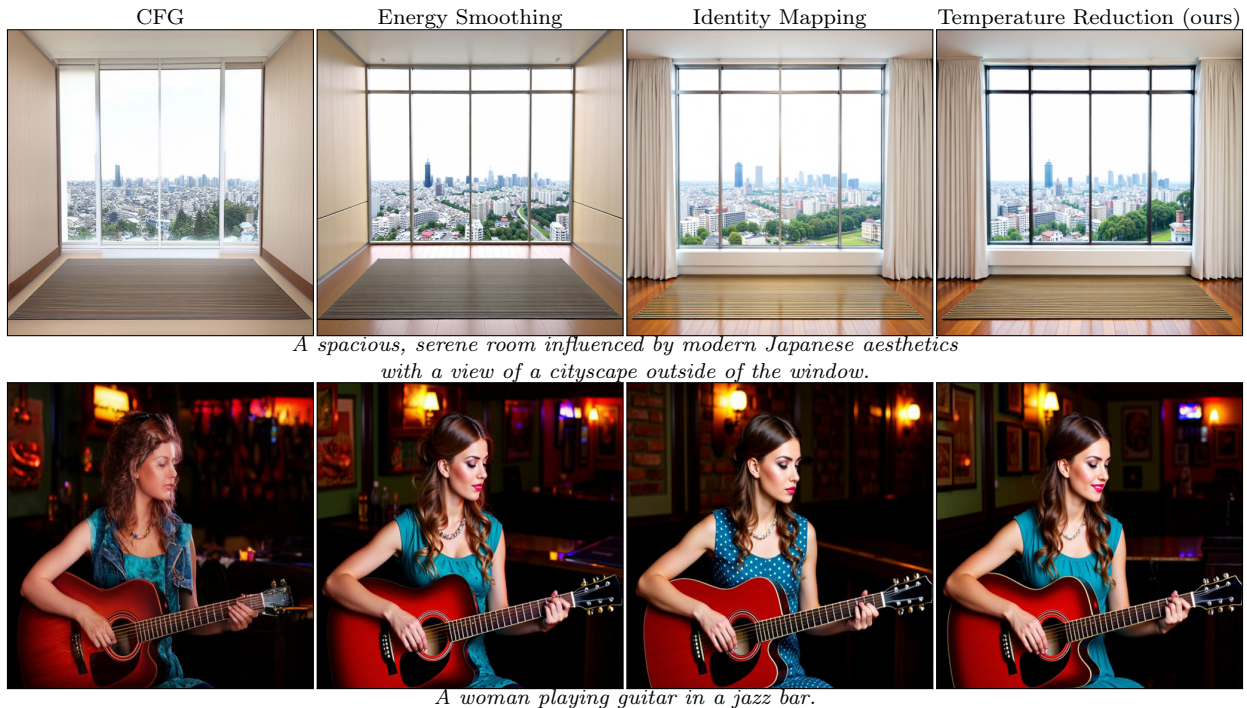


Figure 16 Effect of I-ERG main parameters. We show the effect of applying I-ERG on different layers of the transformer l_{\min}^i, l_{\max}^i . Experiment conducted on DiT-XL/2 model, using a guidance scale of 5.0.



A spacious, serene room influenced by modern Japanese aesthetics with a view of a cityscape outside of the window.

A woman playing guitar in a jazz bar.

Figure 17 Comparing attention rectification mechanisms. Compared to attention smoothing and identity mapping, temperature rescaling better models high-level details in the image such as textures of the tiling and small buildings in the distance. Temperature rescaling also showcases better structural coherence when compared with different methods.

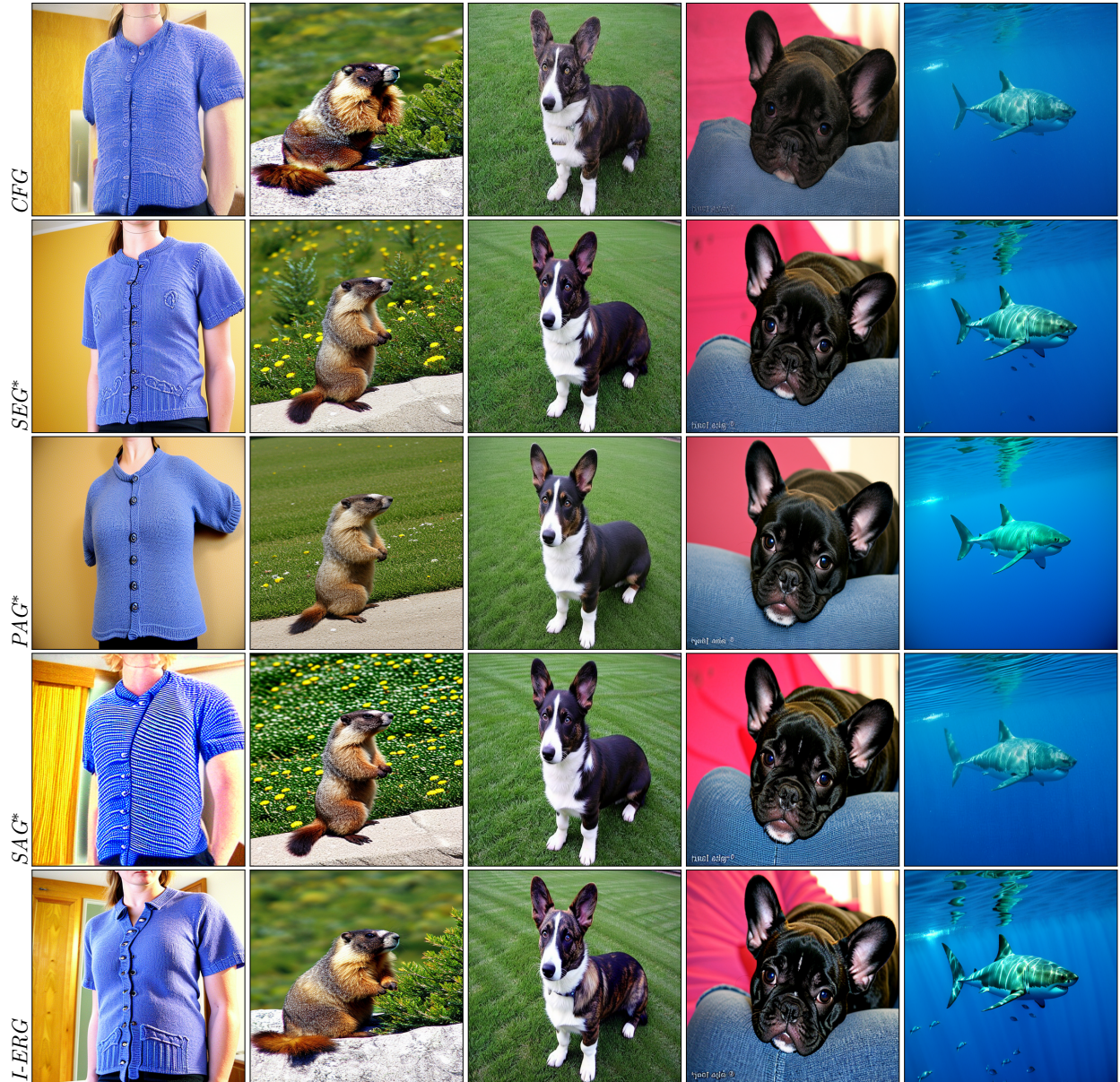


Figure 18 Qualitative comparison on ImageNet-1k@512. Samples from the same column are generated using the same random seed, we compare ERG with CFG and SEG. Our method produces images of better quality. Images generated using Euler sampler with 50 steps.

An elephant crossing a river.



A child wearing an apron and sunglasses posing in front of a blackboard with heart drawings and 'ERG' written in it.



Figure 19 Qualitative example of I-ERG on SD3-medium model compared to standard CFG. We apply our I-ERG on sd3-medium model. We observe better image details using I-ERG (kid's face and details on the blouse in first row. Panda's fur, reflections on the sunglasses in the second row.